POLITECNICO
MILANO 1863

SCUOLA DI INGEGNERIA INDUSTRIALE
E DELL'INFORMAZIONE

Thermal Study of an Innovative Design for Superconducting Dipole Magnet in MgB2 for Energy Saving purposes

TESI DI LAUREA MAGISTRALE IN
NUCLEAR ENGINEERING-INGEGNERIA NUCLEARE

Author: **Simone Busatto**

Student ID:	10573184
Advisor:	Prof. Matteo Passoni
Co-advisor:	Alessio Capelluto, Samuele Mariotto
Academic Year:	2022-23

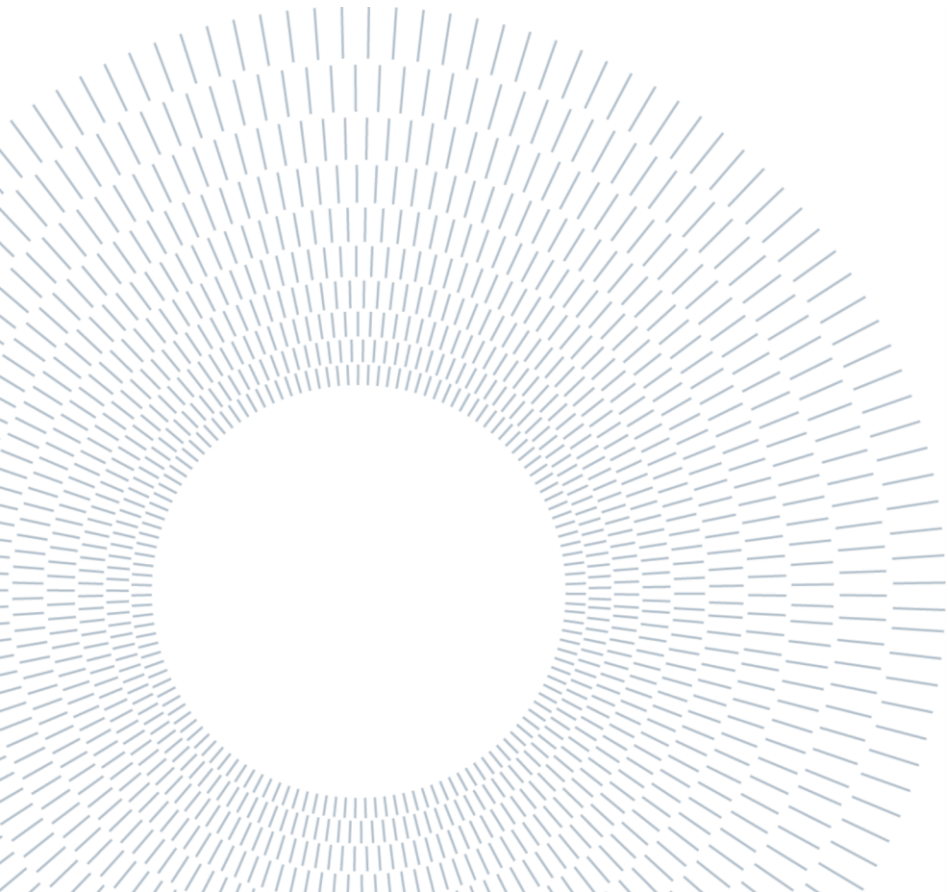

Abstract

In the last years, energy consumption has become a very relevant matter, hence energy savings became a central topic in technological research. For particle accelerator development and diffusion, a critical factor is sustainability. This master thesis presents an analysis of a superconducting magnet (MgB_2 solutions) substituting a normal conducting dipole to reduce the power consumption of the large accelerator facilities, focusing on lowering the consumption of the coils, maintaining the same iron yoke. Thermo-mechanic, alongside magnetic properties, is a key factor in the system and its consumed power. Material properties and dimensions heavily influence the linear power density profile of the coils, which depend on the temperature of the material. Therefore, the precise knowledge of the temperature profile on the coils is very important to model the power consumed by the system. Moreover, the goal of this work is to identify a possible choice for the thermal shield position and material, the tie-rods dimension and positions, coil dimensions, the cryocooler model and the current leads power consumption. As results, it was found a convenient set-up having: 1260 total ropes inside the coil winding; copper thermal shield 5 mm thick, equally distant from the iron yoke (25 mm); G10 tie-rods pre-loaded in a longitudinal crossed configuration with 14 mm radius; brass current leads for the hot head (at 60 K) and superconducting ones for the cold head (10 K); two sided cooling using four PT815 Cryomech's cryocoolers for the coils-thermal shield and two PT805 cryocoolers for the currents leads. This design, depending on the work ratio, can lower the power consumption averaged over a year. With a duty cycle below 53% on the whole year, the power consumption results lower than 30 kW assumed a DC operation mode. Further analyses are suggested, including a more detailed magnetic field analysis and its influence, different material for the magnet and a cost-efficiency analysis.

Keywords: Superconducting Magnet, Dipole Magnet, MgB2, Energy Savings, Dry Magnet

Abstract in lingua italiana

Negli ultimi anni, il consumo di energia è diventato un tema molto rilevante, pertanto il risparmio energetico è diventato un argomento centrale nella ricerca tecnologica. Per lo sviluppo e la diffusione degli acceleratori di particelle, un fattore critico è la sostenibilità. Questa tesi di laurea presenta un'analisi di un magnete superconduttore (in MgB_2) che sostituisce un dipolo a conduzione normale al fine di ridurre il consumo energetico delle grandi strutture degli acceleratori, concentrandosi sul ridurre il consumo delle bobine mantenendo lo stesso supporto in ferro. Le proprietà termo-meccaniche, insieme alle proprietà magnetiche, sono un fattore chiave nel sistema e nel suo consumo di energia. Le proprietà dei materiali e le dimensioni influenzano pesantemente il profilo di densità di potenza lineare delle bobine, che dipende dalla temperatura del materiale. Pertanto, la conoscenza precisa del profilo di temperatura sulle bobine è molto importante per modellare la potenza consumata dal sistema. Inoltre, l'obiettivo di questo lavoro è identificare una possibile scelta per la posizione e il materiale dello schermo termico, le dimensioni e le posizioni dei tiranti, le dimensioni delle bobine, il modello del cryocooler e il consumo di potenza dei cavi di alimentazione. Come risultato, è stato trovato un set-up conveniente che prevede: 1260 corde totali all'interno dell'avvolgimento della bobina; uno schermo termico di rame spesso 5 mm, equidistante dal supporto in ferro (25 mm); tiranti in G10 pre-caricate in una configurazione longitudinale incrociata con un raggio di 14 mm; cavi di alimentazione in ottone per la testa calda (a 60 K) e superconduttori per la testa fredda (a 10 K); raffreddamento su entrambi i lati con quattro cryocooler PT815 di Cryomech per le bobine-schermo termico e due cryocooler PT805 per i cavi di alimentazione. Questo progetto, a seconda del rapporto di lavoro, può ridurre il consumo energetico mediato su un anno. Con un ciclo di lavoro inferiore al 53% durante tutto l'anno, il consumo energetico risulta inferiore a 30 kW assumendo una modalità di funzionamento in corrente continua. Sono suggerite ulteriori analisi, tra cui un'analisi del campo magnetico più dettagliata e la sua influenza, l'utilizzo di materiali diversi per il magnete e un'analisi di efficienza dei costi.

Parole chiave: Magnete superconduttore, Dipolo magnetico, MgB2, Risparmio energetico, Magnete a secco.

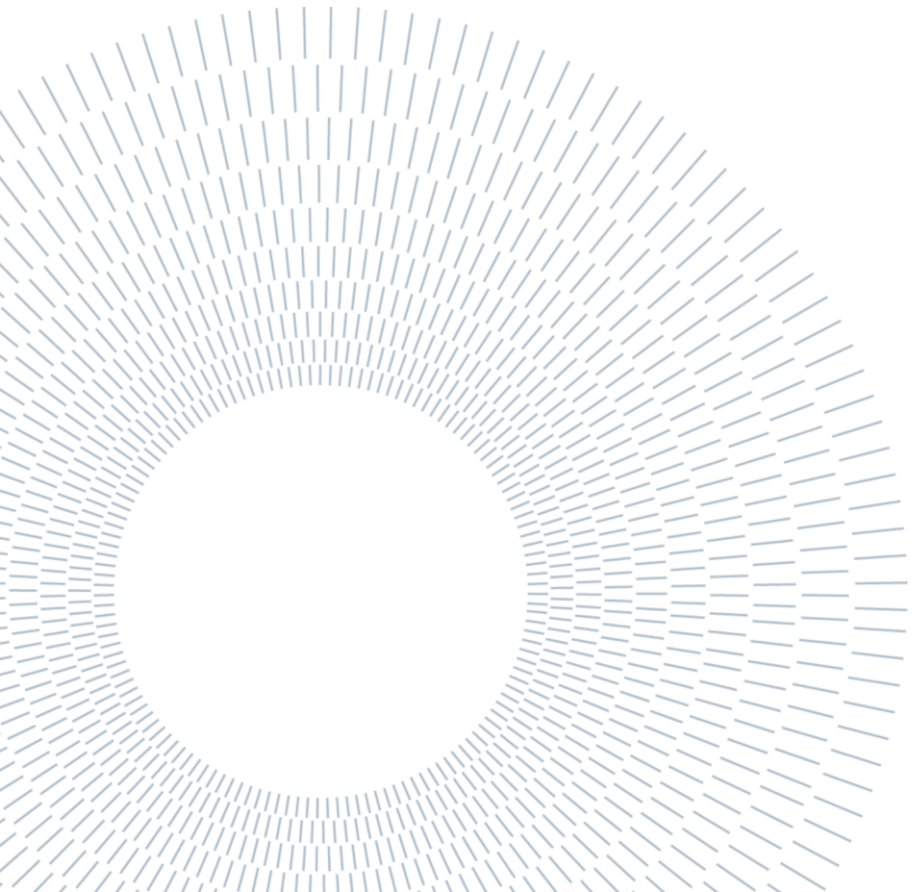

Index

Introduction

For future high-energy physics colliders, sustainability is a critical issue. Designing high-temperature superconducting (HTS) magnets for high field operation temperature of 10-20 K could significantly reduce the power consumption of the cryogenic system in the accelerator facility. For example, in the case of FCC-hh, operating the 15 T dipoles at 20 K instead of the baseline of 2 K could reduce the power consumption of the cryogenic plant [1]. Furthermore, in FCC-ee and in the beamlines of existing large accelerator infrastructures such as CNAO (Pavia), PSI (CH), GSI (DE), and the CERN North Area, the use of superconductivity can dramatically decrease the power requirements of current resistive magnets. Some of these magnets individually consume 200-1000 kW, the required power could be reduced in principle and in certain cases by a factor of 20 to 50. These magnets operate at moderate or low magnetic fields, making them suitable to operate the superconducting equivalent magnet at 10-20 K. Additionally, the magnets used as spectrometers in future experimental detectors (such as Alice) and other similar cases could significantly benefit from using superconducting coils in a low field configuration with the assistance of an iron yoke or poles, commonly referred to as a "superferric" layout. While the high field of FCC-hh requires the use of high-temperature superconductors such as REBCO, the superferric configuration for beamlines or detectors can utilize either REBCO or MgB_2 as HTS coils in a cryogen-free mode, eliminating the need for liquid helium.

This Master Thesis is part of the preliminary analysis of the project ESABLIM (**E**nergy **S**aving **A**ccelerator and **B**eam **Li**ne **M**agnets) by the University of Milan and INFN-LASA, with the partnership of ASG Superconductors, leading company in MgB_2 magnets and main supervisor of this study [2].

Following the knowledge gain during the Master in Nuclear Engineering on the thermo-mechanical analysis of a fission reactor and on magnetic properties and use of the materials, the study in this thesis work will examine the case of low-moderate field magnets, tackling magnetic, thermal and mechanical issue in designing a superconducting dipole magnet for energy saving. The models here applied for particle accelerators can be used in many applications where a low magnetic field is required over a long length and period of time in a dry magnet, such as magnetic

confinement in nuclear fusion. Superconducting magnets are crucial for confining and controlling plasma in experimental fusion reactors. They produce the strong magnetic fields required to confine and stabilize plasma, enabling the study and development of fusion energy as a potential clean and sustainable energy source. Moreover, MgB_2 magnet can be used in several nuclear techniques such as: Magnetic Resonance Imaging (MRI), where a strong and stable magnetic field is required. The magnets enable detailed imaging of internal body structures and aid in the diagnosis of various medical conditions; Nuclear Magnetic Resonance (NMR) Spectroscopy: where the magnet produces the homogeneous magnetic fields necessary for precise measurement and analysis of nuclear spin interactions.

This Master Thesis is structured in five chapters, each focusing on an important aspect of the study. The first two chapters have a theoretical approach on two important aspects: the materials properties at cryogenic temperatures and the superconducting nature of the magnet. The third chapter focused on the goal and technological components of the system, then in the following chapter the model created to optimize magnet configurations and design will be analyzed and the results obtained discussed. The last chapters focused on the conclusions reached after this study and some possible future developments.

1. Material properties at Cryogenic Temperatures

From room temperature down to cryogenic temperatures. materials properties vary significantly and have different behaviors when temperature changes and the various phenomena that characterize the different properties have not the same importance.

In this chapter the various properties of the materials utilized are analyzed and some common material Data will be provided.

1.1 Thermal Properties

While working at low temperatures it is very important to analyze and consider the materials behaviors when is present a heat flow (due to the difference of temperature with the ambient), heat generation and any other temperature gradient induced by internal or external sources.

The thermal (and electrical) properties of any material are related to the vibrations of its atoms around their equilibrium positions (in a lattice crystal). The amplitude of these vibrations depends on temperature and diminishes as the temperature decreases. Thermal properties also depend on the movements of negative charges (electrons) and positive charges (vacancies) if the material is a conductor.

1.1.1 Thermal capacity

The heat capacity C is defined as the quantity of energy (heat) that must be absorbed by the material to increase its temperature T by 1 K [3] given its mass m. The unit of this extensive quantity is $[J/K]$. The intrinsic property of each material is given by the specific heat c, which is described by the heat capacity or thermal capacity per unit of mass $[J/K\ Kg]$. The heat capacity of a material is thus its ability to store or release heat energy.

It is an important property in cool-down or working processes used in the estimation of the energy (and cost) involved, and in the assessment of the transient states of the heat transfer. As the temperature tends to zero, so does the heat capacity.

Heat can be supplied at constant volume V or constant pressure p, defining two heat capacities such that:

$$C_v = T\left(\frac{\partial S}{\partial T}\right)_V = \left(\frac{\partial U}{\partial T}\right)_V, C_p = T\left(\frac{\partial S}{\partial T}\right)_p = \left(\frac{\partial H}{\partial T}\right)_p \quad (1.1)$$

where S is the entropy, U is the internal energy, and H is the enthalpy (all expressed in joules).

For a system comprising the association of several homogenous materials i each having a mass m_i :

$$C_v = \sum_i m_i c_{v_i} \text{ and } C_p = \sum_i m_i c_{p_i} \quad (1.2)$$

For solids at low temperatures, the difference between the two values is negligible (less than 1%), and thus no distinction will be made in the following between C_v and C_p [4].

Heat capacity of the materials

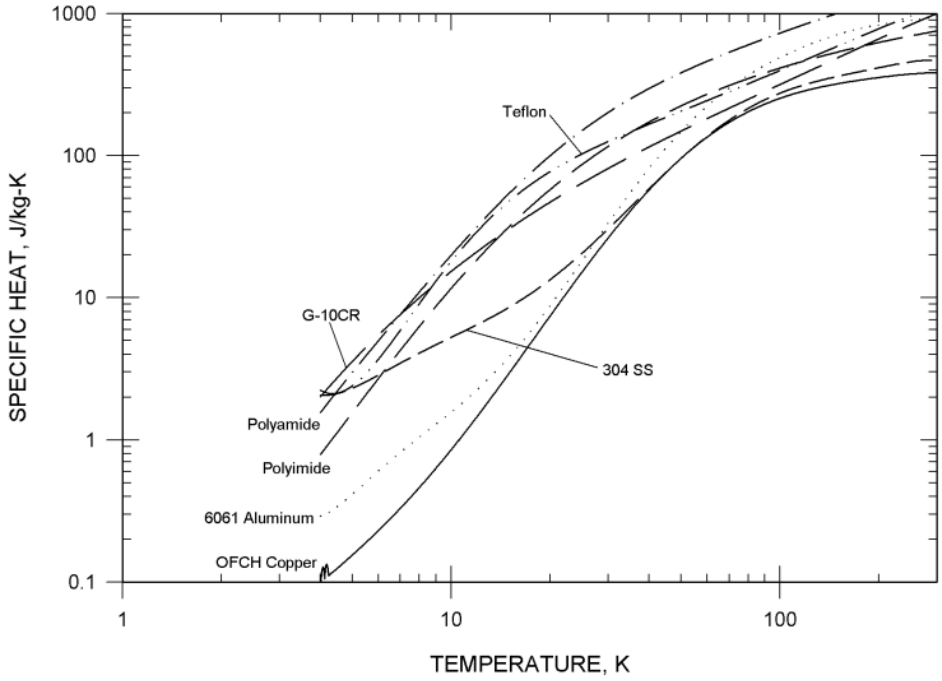

Figure 1.1: Specific heat of different materials [5]

The type of material (metal, semiconductor or insulator) will change the nature of the heat capacity, because it is composed of a crystal contribution and a free electron one. Hence, metals will be highly influenced by the free electrons unlike insulators.

Crystal lattice contributions

It is possible to consider the sum of the energy of all phonon modes and apply the Debye theory [6], for which the velocity of sound is taken as constant for each polarization type, in a similar way as it would be for a classical elastic continuum.

once all the values of phonon internal energy are added, up to a cut-off frequency ω_D [7], we obtain the total phonon energy U_{ph}.

$$U_{ph} = 9Nk_BT\left(\frac{T}{\theta}\right)^3 \int_0^{\theta/T} dx\ \frac{x^3}{e^x - 1} \tag{1.3}$$

With $\theta \equiv \frac{\hbar\,\omega_D}{k_B} = \frac{\hbar\,v}{k_B}\left(\frac{6\pi^2 N}{V}\right)^{1/3}$ the Debye temperature and where $k_B = 1.38 \cdot 10^{-23}\ \frac{J}{K}$ is the Boltzmann constant, $\hbar = 1.055 \cdot 10^{-34}\ J \cdot s$ is the reduced Plank constant, v the constant velocity of sound and $\frac{N}{V}$ the number of atoms per volume of material.

The heat capacity is found easily by differentiating the expression (1.3) with respect to temperature. Then

$$C_v = 9Nk_B\left(\frac{T}{\theta}\right)^3 \int_0^{\theta/T} dx\ \frac{x^4 e^x}{(e^x - 1)^2} \tag{1.4}$$

At very low temperatures we may approximate (1.3) by letting the upper limit go to the infinity. We have $U \cong 3\pi^4 N k_B\, T^4/5\theta^3$ for $T \ll \theta$, and

$$C_v \cong \frac{12\pi^4}{5} N k_B \left(\frac{T}{\theta}\right)^3 \cong 234\, N k_B \left(\frac{T}{\theta}\right)^3 \tag{1.5}$$

Which is the *Debye T^3 approximation*.

Free electrons contributions

Thermal excitation induced by heating concerns only a fraction of the electrons for which the energy is within k_BT of the Fermi energy, $E_F = \frac{\hbar}{2m_e}\left(\frac{3\pi^2 N}{V}\right)^{2/3}$ where $m_e = 9.109 \cdot 10^{-31} Kg$ is the mass of an electron [6]. The total energy of the electrons is:

$$U \approx \frac{N\,T}{T_f} k_B T \tag{1.6}$$

where $T_F = E_F/k_B$ is called the *'Fermi temperature'*.

The electronic heat capacity given by the free-electron-gas model thus evolves linearly with respect to the temperature:

$$C_v = \frac{\partial U}{\partial T} \approx \left(\frac{T}{T_F}\right) N k_B \tag{1.7}$$

At temperatures much lower than the Fermi temperature, the heat capacity (of free electrons) can be expressed by

$$C_v = \frac{1}{2}\pi^2 \left(\frac{T}{T_F}\right) N k_B \tag{1.8}$$

1.1.2 Thermal conductivity

Thermal conductivity can be defined as the rate at which heat flows through a specified material. It is expressed as the amount of energy variation per unit time through a unit area with a temperature gradient of one degree per unit distance.

Thermal conductivity implies the presence of thermal conduction which is the principal heat transfer method present in superconducting magnet support system alongside heat irradiation.

The *Fourier equation* couples the thermal conductivity with the thermal gradient and the heat diffusing through a unit surface in a unit time.

$$\overrightarrow{\dot{Q}''} = -k\overrightarrow{\nabla T} \left[\frac{W}{m^2}\right] \tag{1.9}$$

As an example, and first approximation, we can consider a linear [8](one-dimensional) support with length L, cross-section A and with its ends at temperature T_{cold} and T_{hot}, respectively the coldest and hottest temperatures of the support. Applying the eq. (1.9), and considering the cross-section constant along the whole length of the support, we obtain

$$\int_0^L \frac{\dot{Q}}{A} dx = -\int_{T_{cold}}^{T_{hot}} k \, dT \tag{1.10}$$

If k doesn't depend on the temperature the equation become $\frac{\dot{Q}}{A} L = -k(T_{hot} - T_{cold})$, this means that the heat diffuses from the higher to the lower temperature. However, thermal conductivity depends on temperature, especially in the cryogenic domain,

leading to a nonlinear profile. Thermal conductivity can be easily considered as the sum of two main contributions, heat transported by electrons and by lattice vibrations or phonons $k = k_{ph} + k_e$.

Crystal lattice contributions to the thermal conductivity

If c is the heat capacity of a particle, then in moving from a region at local temperature $T + \Delta T$ to a region at local temperature T a particle has to lower its energy by the factor $c\Delta T$ in the interaction with the local material. Now ΔT, between the ends of the particle free path without collisions with the material lattice is given by:

$$\Delta T = \frac{dT}{dx} l_x = \frac{dT}{dx} v_x \tau \tag{1.11}$$

Where τ is the average time between collisions.

The net flux of energy (from both sense of the particle flux) is therefore:

$$\dot{Q}'' = -n\langle v_x^2 \rangle c\tau \frac{dT}{dx} = -\frac{1}{3} n\langle v^2 \rangle c\tau \frac{dT}{dx} \tag{1.12}$$

If, as for phonons, v is constant, we may write (1.12) as

$$\dot{Q}'' = -\frac{1}{3} Cv\tau \frac{dT}{dx} \tag{1.13}$$

With $l \equiv v\tau$ [9] and $C \equiv nc$. Thus $k_{ph} = \frac{1}{3} Cvl$.

Free electrons contributions to the thermal conductivity

The thermal conductivity of a Fermi gas follows from (1.8) for the heat capacity considering the *Wiedemann–Franz law* [10] and with $\epsilon_F = \frac{1}{2} m v_F^2$:

$$k_{el} = \frac{\pi^2}{3} \frac{n k_B^2 T}{m v_F^2} \cdot v_F \cdot l = \frac{\pi^2 n k_B^2 T \tau}{3m} \tag{1.14}$$

Here $l = v_F \tau$; the electron concentration is n, and τ the collision time.

In pure metals the electronic contribution is dominant at all temperatures. In impure metals or in disordered alloys, the electron mean free path is reduced by collisions with impurities, and the phonon contribution may be comparable with the electronic contribution.

Integrals of the thermal conductivities

As explained in the previous sections, because the thermal conductivity depends on temperature, especially in the cryogenic domain, the integration of the local thermal

conductivity as function of the temperature must be considered in order to evaluate the diffusive heat flux between two local temperatures (see Eq. (1.10)). Hence, for engineering purposes, it is convenient to provide integrals of the thermal conductivities evaluated from a reference temperature T_{ref}. The integral can thus be evaluated by subtraction:

$$\int_{T_1}^{T_2} k\, dT = \int_{T_{ref}}^{T_2} k\, dT - \int_{T_{ref}}^{T_1} k\, dT \tag{1.15}$$

Thermal conductivity of the materials

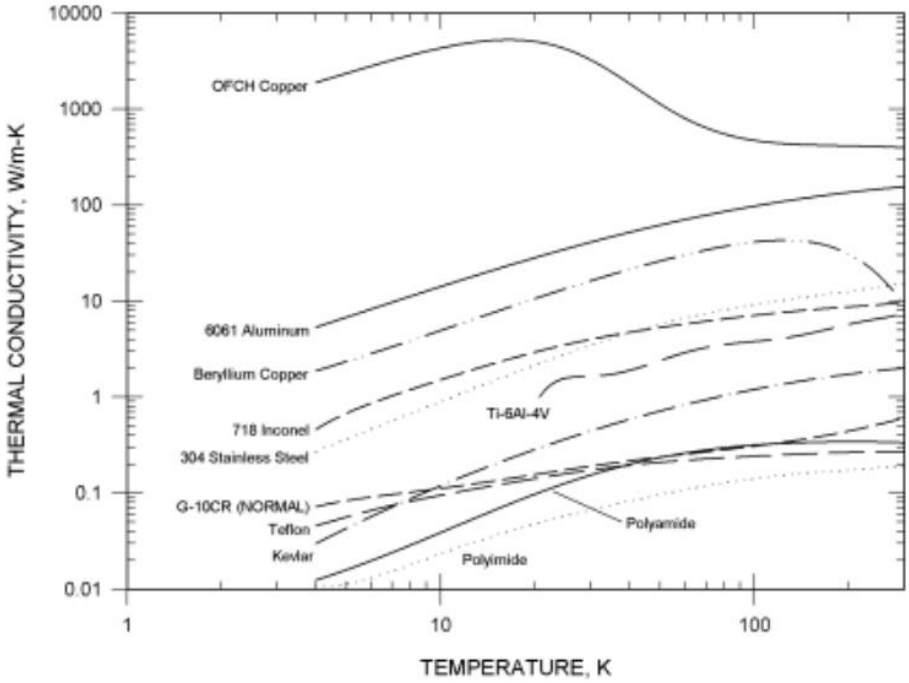

Figure 1.2: Thermal conductivity of various materials [5]

At cryogenic temperature pure metal will have the highest thermal conductivity, especially highly pure aluminum and copper. Instead, organic components and plastic will have a very low thermal conductivity and hence will tend to heat faster.

1.2 Electrical properties

1.2.1 Electrical resistivity for metals

For metallic conductors, electric charges e are transported by n 'free electrons', in a constant electric field $\vec{E}$, the electric current density is:

$$\vec{j} = nq\vec{v} = \frac{ne^2\tau}{m_e}\vec{E} \tag{1.16}$$

This is *Ohm's law*. The electrical conductivity was defined as $\vec{j} = \sigma\vec{E}$ from Gustav Kirchhoff [11], so by (1.16)

$$\sigma = \frac{ne^2\tau}{m_e} \tag{1.17}$$

where m_e is the mass of an electron and τ describes the free time during which the field acts on the electrons. The electrical resistivity ρ is defined as the reciprocal of the conductivity, so that:

$$\rho = \frac{m_e}{ne^2\tau} \tag{1.18}$$

The electrical resistivity of most metals is dominated at room temperature by collisions of the conduction electrons with lattice phonons and at liquid helium temperature by collisions with impurity atoms and mechanical imperfections in the lattice. The rates of these collisions are often independent to a realistic approximation, so when the electric field is switched off the momentum distribution of the electrons would relax back to its ground state with the net relaxation rate: $\frac{1}{\tau} = \frac{1}{\tau_L} + \frac{1}{\tau_i}$, where τ_L and τ_i are the collision times for scattering by phonons and by impurities, respectively [6].

The net resistivity is given by:

$$\rho = \rho_L + \rho_i \tag{1.19}$$

Where ρ_L is the resistivity caused by the thermal phonons, and ρ_i is the resistivity caused by scattering of the electron waves by static defects that disturbes the periodicity of the lattice. This independence is expressed by *Matthiessen's rule*.

The residual resistivity, $\rho_i(0)$, is the extrapolated resistivity at 0 K because the lattice contribution vanishes for $T \to 0$. The lattice resistivity, $\rho_L(T) = \rho - \rho_i(0)$, is the same for different samples of a metal, even though the residual resistivity may itself vary widely. $\rho_L(T)$ depends on the frequency of the collisions of electrons with thermal phonons (and electrons) [12]. For $T > \theta$, the concentration of phonons is proportional to the temperature, and so $\rho_L \propto T$ and thus $\rho \propto T$. As $T \to 0$, $\rho \to \rho_i$, with ρ_i proportional to T^n (with $1 < n < 5$ [6], [13]). An indication of the impurities and crystallographic defects in a metal (imperfections) is provided by the determination of the Residual (electrical) Resistivity Ratio (RRR) defined as the ratio of its resistivity at

room temperature to its residual resistivity. Therefore, the smaller the imperfection content in a material, the larger the RRR is.

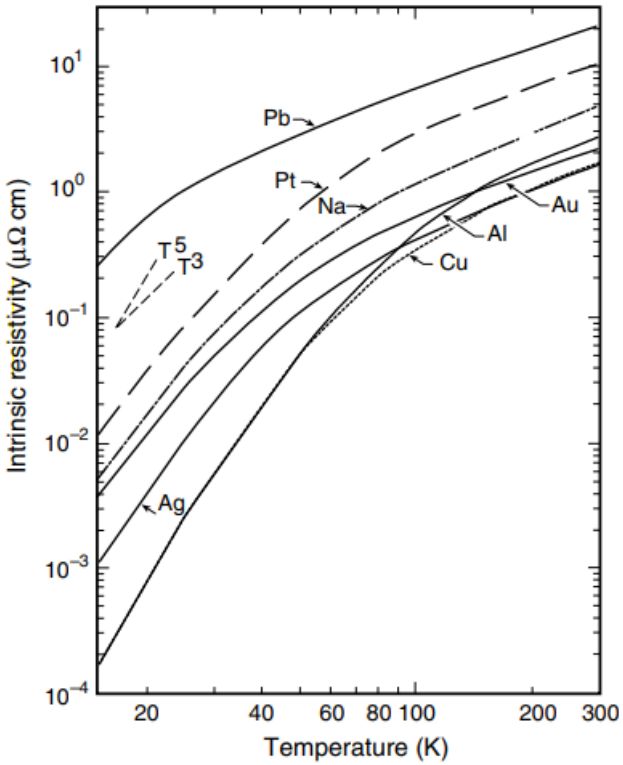

Figure 1.3: Electrical resistivity of ideally pure metals [14].

Ratio of thermal to electrical conductivity

The *Wiedemann-Franz law* [10] states that for metals at not too low temperatures the ratio of the thermal conductivity to the electrical conductivity is directly proportional to the temperature with the value of the constant of proportionality independent of the metal.

$$\frac{k_e}{\sigma} = \frac{\pi^2}{3}\left(\frac{k_B}{e}\right)^2 T = 2.445 \cdot 10^{-8} \cdot T \tag{1.20}$$

Thus, the purer a material is, the larger its electronic thermal conductivity.

1.2.2 Electrical conductivity for semiconductors

For semiconductors, electric charges are transported by conduction band electrons and holes in the valence band. Around the ambient temperature, lattice vibrations are predominant and electrical properties are not modified by impurities. The electrical resistivity can be expressed as $\rho(T) = a \cdot e^{\delta/2k_BT}$, where a is an experimental constant

and δ is the energy band depending on the material [15]. At low temperatures, lattice vibrations are negligible and impurities play an important role in the transport of charges. Thus, the resistivity of semiconductors is very non- linear: it typically increases as temperature drops due to there being fewer electrons in the conduction band.

1.3 Mechanical properties

In solids, atoms are in equilibrium positions depending on their interaction energies. Moving them from their equilibrium positions requires imposing an external force to overcome the restoring force. For small displacement amplitudes, the restoring force can be considered as proportional to this elastic deformation, and the equilibrium position is recovered if the external force is removed. For a larger displacement (larger external force), a limited number of atomic bonds break. Those dislocations enable atoms in specific crystal planes to slip one from another, yielding a permanent plastic deformation that propagates within the material along the packed planes of atoms because the (shear) stress needed to move increases with the spacing between the planes.

Any material or structure may fail when it is overloaded. The successful design of a structure requires detailed structural and stress analysis in order to assess whether it can safely support the required loads or not. It is important to introduce some important concepts.

- *Force:* A force is a measure of its tendency to cause a body to move or translate in the direction of the force. A complete description of a force includes its magnitude and direction. The magnitude of a force acting on a structure is usually measured by Newton (N).
- *Stress:* Stress can be defined as the intensity of internal force that represents internal force per unit area at a point on a cross-section. Stresses are usually different from point to point. There are two types of stresses, namely normal and shear stresses. Normal stress is a stress perpendicular to a cross-section or cut. Shear stress is a stress parallel to a cross-section or cut.
- *Strain:* Strain is a measure of relative deformation. Strains can be categorized as normal and shear strains. Normal strain is a measure of the change in length per unit length under stress. Shear strain is a measure of the change caused by shear stresses in the right angle between two fibers within a plane.

$$\sigma = \frac{F}{S}; \varepsilon = \frac{\Delta L}{L_0} \tag{1.21}$$

Plotting the stress dependence on the strain is possible to evidence two domains.

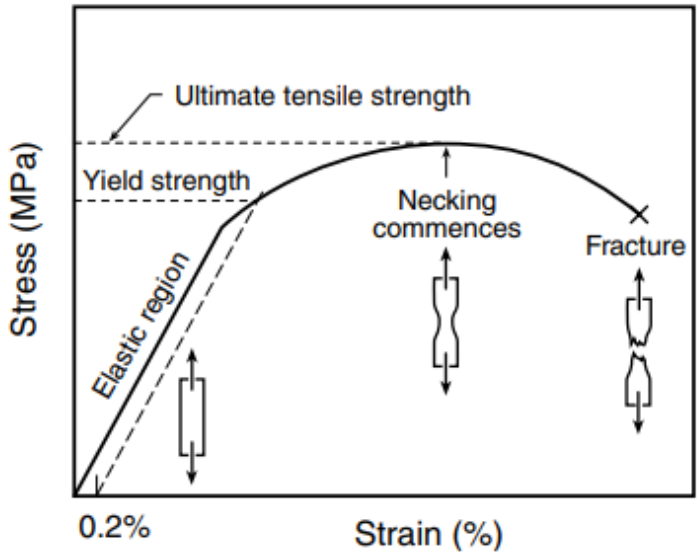

Figure 1.4: Stress–strain curve for ductile materials when stressed axially.

1.3.1 Elastic domain

In the elastic domain, the elongation is proportional to the tensile force (*Hooke's law*), and the sample can reversibly recover its initial size by removing the force. The proportional coefficient is the Young modulus (modulus of elasticity) defined as: $E = \frac{\sigma}{\varepsilon}$; it is a measure of the stiffness of the material and is used in computing structural deflections. The modulus of elasticity is determined by the binding forces between atoms and is thus generally not affected by impurities within the lattice crystal (chemical additions to obtain alloys, for example). However, temperature does affect these forces due to the thermal excitation of the lattice: the modulus of elasticity is slightly larger at low temperature than around ambient and drops at high temperature [16].

The elastic limit or yield stress, σ_{yield}, is the tensile stress from which elongation of the sample begins to increase disproportionately with increasing tensile force. A plastic elongation remains after the removal of the force. The yield point is not always a sharply defined point, especially for hard material. For engineering purposes, offset yield strengths are often used: they are the tensile stresses from which a permanent plastic deformation of 0.1%, 0.2% or 0.5% remains. The yield strength generally increases at low temperature [13].

1.3.2 Plastic Domain

The ultimate strength is the maximum tensile stress a material can withstand (under uniaxial loading), but it is not often used in practice. A material is said to be ductile when it can be plastically deformed without breaking. While, otherwise, it is said to be brittle. Ductility allows a material to be submitted to metal working without breaking and provides a security margin when excess loading is applied to the material. It can be assessed by measuring the elongation and cross-section at fracture. The ductility of metals and metallic alloys depends on their crystal structure and temperature. Materials with a face-centered cubic (f.c.c.) crystal structure (such as Cu-Ni alloys, aluminum and its alloys, austenitic stainless steel, Ag, Pb, brass, Au, Pt, Inconel), are ductile even at low temperatures. Thus, they are favored in cryogenics applications, as ductility provides some safety margin from rupture. For materials with a body-centered cubic (b.c.c.) crystal structure (ferritic steels, carbon steel, teel with Ni < 10%, Mo, Nb, Cr, Nb–Ti), a ductile–brittle transition appears at low temperature: the plasticity capacity is wiped out. The toughness of a material describes its ability to absorb energy and plastically deform until fracture. A tough material can withstand occasional stresses above the yield stress without fracturing. As the temperature decreases, both toughness and fracture toughness decrease.

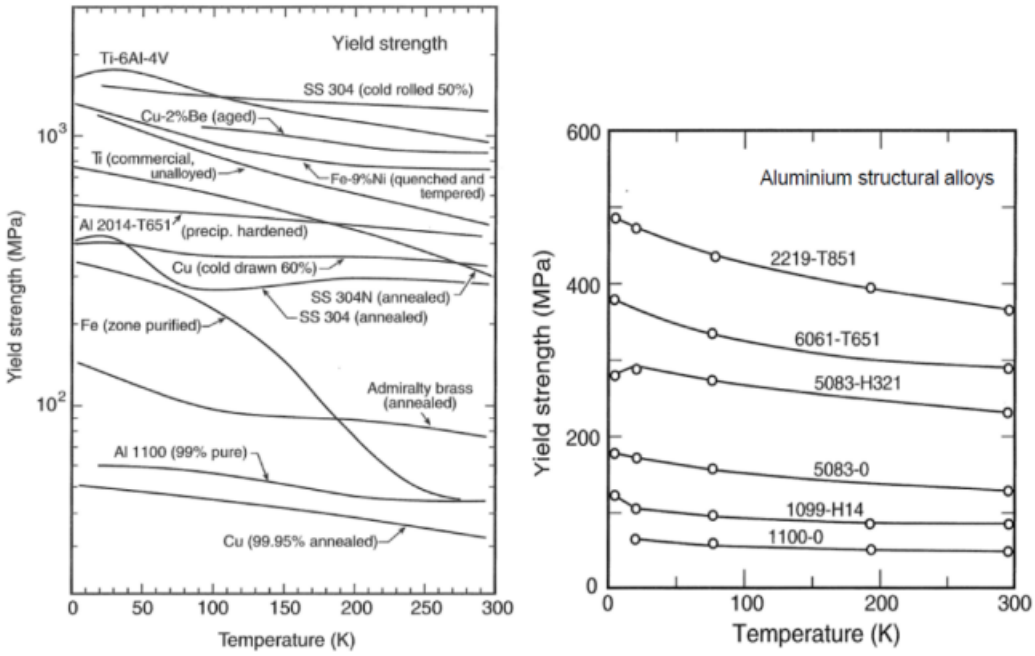

Figure 1.5: Yield strength of different materials [13].

1.3.3 Buckling

Compression members, such as columns, are mainly subjected to axial compressive forces. The stress on a cross-section is therefore normal compressive stress. A short column usually fails due to yielding or shearing, depending on material properties of the column. However, when a compression member becomes longer, it could become laterally unstable and eventually collapse through sideways buckling at an axial compression. The compressive load could be far smaller than the one that would cause material failure of the same member. A lateral deflection from the original position will be observed when the applied compression reaches a certain value, which is designated P_{cr} and called critical buckling load. The critical buckling load is the maximum load that can be applied to a column without causing instability. Any increase in the load will cause the column to fail by buckling. At the critical buckling load, a column may buckle or deflect in any lateral direction. In general, the flexural rigidity or stiffness of a column is not the same in all directions. By common sense, a column will buckle (deflect) in a direction related to the minimum flexural rigidity, EI, that is, the minimum second moment of area of the cross-section.

For a column with pinned ends using the *Euler formula* we can derive the value of P_{cr}.

$$P_{cr} = \frac{\pi^2 EI}{L^2} \tag{1.22}$$

This is a very important constraint when building thin pieces like tie-rods as we while see in the design of the vacuum chamber.

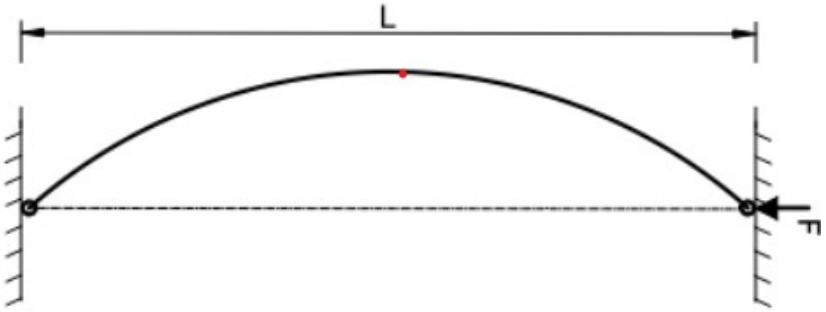

Figure 1.6: Possible buckling failure.

1.4 Magnetic properties

In a vacuum, the magnetic field $\vec{B}$ (unit: $T \equiv V \cdot s \cdot m^{-2} \equiv N \cdot A^{-1} \cdot m^{-1}$) is proportional to the excitation magnetic field $\vec{H}$ (unit: $V \cdot s \cdot A^{-1} \cdot m^{-1} \equiv A \cdot m^{-1}$): $\vec{B} = \mu_0 \vec{H}$, the proportional factor being the permeability of free space $\mu_0 = 4\pi \cdot 10^{-7}\ H/m$. In a material, $\vec{B} = \mu_0(\vec{H} + \vec{M})$, where $\vec{M} = \chi \vec{H}$ is the magnetization and represents

how strongly a region of material is magnetized by the application of $\vec{H}$. It is the net magnetic dipole moment per unit volume. Thus, $\vec{B} = \mu_0(1 + \chi)\vec{H} = \mu_0\mu_r\vec{H}$, where μ_r is the relative magnetic permeability. The magnetic moment of a free atom depends on electron spin, the orbital kinetic moment of the electrons around the nucleus, and the kinetic moment change induced by the application of a magnetic field. Five types of magnetic behaviors can be distinguished: diamagnetism and paramagnetism, which are induced by isolated atoms (ions) and free electrons, and ferromagnetism and antiferromagnetism, which occur due to the collective behavior of atoms [17].

Here we will mainly focus on ferromagnetism due to the active role of the iron yoke in the generation of the magnetic field. It is important to notice that it can be neglected the superconductor's diamagnetism because it involves small magnetic field corrections at the center of the magnet.

1.4.1 Ferromagnetism

For ferromagnetic materials, such as Fe-Ni-Co alloys (not austenitic steels), magnetization is due to the contribution of the unpaired electron spins and coupling interactions causing magnetic moments of adjacent atoms to be parallel to an applied magnetic field and parallel to each other. Thus, magnetization remains. It is important to notice that ferromagnetic materials spontaneously divide into magnetic domains because the exchange interaction is a short-range force, so over long distances of many atoms the tendency of the magnetic dipoles to reduce their energy by orienting in opposite directions wins out. Hence, in a strong magnetic field the one orientating are the grains or domains. Above the Curie temperature θ_C, which is generally larger than the ambient temperature, the *Curie–Weiss law* yields a paramagnetic behavior: $\chi = constant/(T - \theta_c)$. Below θ_C, $(M(0) - M(T)) \,/\, M(0) \propto T^{3/2}$. When an increase in the applied external magnetic field H cannot augment the magnetization M, the material reaches its saturation state.

	Fe	Co	Ni	Gd	CrO_2	EuO
Curie T [K]	1043	1388	627	292	386	69

Table 1.1: Curie temperature of different materials.

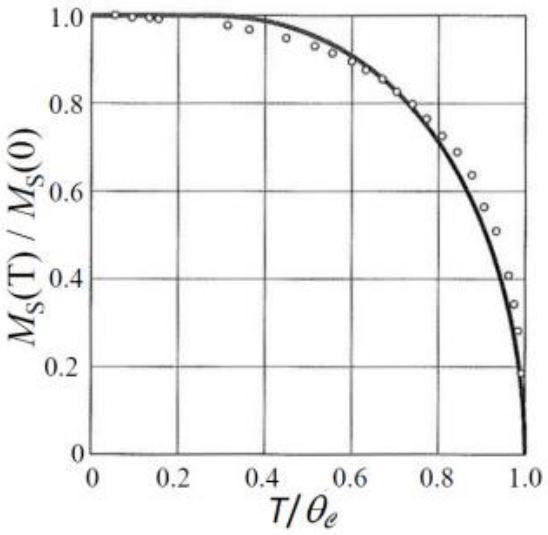

Figure 1.7: Magnetization at saturation of nickel as a function of temperature [6].

1.4.2 Eddy currents

Eddy currents are loops of electric current induced within conductors by a varying in time magnetic field in the conductor according to *Maxwell-Faraday equation*:

$$\nabla \times \vec{E} = -\frac{\partial \vec{B}}{\partial t} \tag{1.23}$$

These currents flow in closed loops within conductors, in planes perpendicular to the magnetic field. The magnitude of the current in a given loop is proportional to the strength of the magnetic field, the area of the loop, and the rate of change of flux, and inversely proportional to the resistivity of the material. From the *Lenz's law* [18], an eddy current creates a magnetic field that opposes the change in the magnetic field that created it, and thus eddy currents react back on the source of the magnetic field. Hence, in the presence of a varying magnetic field, in normal resistive materials, there will be also power depletion.

2. Superconductivity

For most metals the resistivity does indeed behave as (1.19) at low temperatures. However, for a superconductor something dramatically different happens [19]. Upon cooling the resistivity first follows the simple smooth behavior, but then suddenly vanishes entirely. The temperature where the resistivity vanishes is called the critical temperature, T_C. Below this temperature the resistivity is not just small, but is, as far as can be measured, exactly zero. This phenomenon was a complete surprise when it was first observed by H. Kammerling Onnes in 1911 [20]. He wanted to test the validity of the *Drude theo*ry by measuring the resistivity at the lowest temperatures possible. The first measurements on samples of platinum and gold were quite consistent with the *Drude model*. But then he turned his attention to mercury, because of its especially high purity. Based on (1.19) one could expect a very small, perhaps even zero, residual resistivity in exceptionally pure substances. But what Kammerling Onnes observed was completely unexpected, and not consistent with (1.19). Surprisingly he discovered that all signs of resistance appeared to suddenly vanish suddenly below about 4K. This was quite unexpected from the *Drude model*, and was, in fact, the discovery of a new state of matter: superconductivity [21].

2.1 Superconducting materials

Several elements in the periodic table become superconducting at low temperatures. Of the elements, Niobium (Nb) has the highest critical temperature T_C of $9.2K$ at atmospheric pressure (it is one of the few pure elements that is a type II superconductors [22]). Interestingly, some common metals such as aluminum ($1.2K$), tin ($3.7K$) and lead ($7.2K$) become superconducting, while equally good, or better, metals (such as copper, silver or gold) show no evidence for this state of the matter. It is still a matter of debate whether they would eventually become superconducting or not if made highly pure and cooled to sufficiently low temperatures. Recently was discovered that quite a few more elements also become superconducting when they are subjected to extremely high pressures. Samples must be pressurized between two anvil shaped diamonds. Using this technique, it is possible to obtain such high

pressures that substances which are normally insulators become metallic, and some of these novel metals become superconducting [23]. Sulphur and oxygen both become superconducting at surprisingly high temperatures. Even iron becomes superconducting under pressure. At normal pressures iron is, of course, magnetic, and the magnetism prevents superconductivity from occurring. However, at high pressures a non-magnetic phase can be found, and this becomes superconducting.

Superconductivity appears to be common in nature, and there are perhaps several hundred known superconducting materials. Before 1986 the highest known T_C values were in the A-15 type materials, including Nb_3Ge with $T_C = 23K$. This, and the closely related compound Nb_3Sn ($T_C = 18K$) are widely used in the superconducting magnet industry.

In 1986 Bednorz and Muller discovered that the material $La_{2-x}Ba_xCuO_4$ becomes superconducting with a T_C which is maximum at *38K* for x ≈ 0.15 [24]. Within a matter of months, the related compound $YBa_2Cu_3O_7$ was discovered to have $T_C = 92\,K$, ushering in the era of 'high temperature superconductivity'. This breakthrough was especially important in terms of possible commercial applications of superconductivity, since these superconductors are the first which can operate in liquid nitrogen (boiling point *77K*) rather than requiring liquid helium (*4K*). As well as high temperature superconductors, there are also many other interesting superconducting materials. Some of these have exotic properties which are still not understood and are under very active investigation. These include other oxide-based superconducting materials, organic superconductors, and 'heavy fermion' superconductors.

2.2 Zero-resistivity

In superconductors the resistivity, ρ, becomes zero, and so the conductivity σ appears to become infinite below T_C. To be consistent, to have a finite current density, following $\vec{j} = \sigma\vec{E}$ we must always have zero electric field, $\vec{E} = 0$, at all points inside a superconductor. We have current flow without electric field. Notice that the change from finite to zero resistivity at the superconducting critical temperature T_C is very sudden.

This represents a thermodynamic phase transition from one state to another. As for other phase transitions, such as from liquid to gas, the properties of the phases on either side of the transition can be completely different. The change from one to the other occurs sharply at a fixed temperature rather than being a smooth cross-over from one type of behavior to another. Here the two different phases are referred to as the "normal state" and the "superconducting state". In the normal state the resistivity and

other properties behaves similarly to a normal metal, while in the superconducting state many physical properties, including resistivity, are quite different. In some cases, notably the high temperature superconductors, looking closely at the $\rho(T)$ curve near to T_C shows a small range of temperatures where the resistance starts to decrease before becoming truly zero. This bend is due to thermodynamic critical fluctuations associated with the phase transition. The precise thermodynamic phase transition temperature T_C can be defined as the temperature where the resistivity first becomes exactly zero. The key characteristic of the superconducting state is that the resistivity is exactly zero,

$$\rho = 0 \tag{2.1}$$

or the conductivity σ, is infinite.

The most convincing evidence that superconductors really have $\rho = 0$ is the observation of persistent currents. If we have a closed loop of superconducting wire, then it is possible to set up a current, *I*, circulating in the loop. Because there is no dissipation of energy due to finite resistance, the energy stored in the magnetic field of the ring will remain constant and the current never decays. To see how this persistent current can be set up, consider the flux of magnetic field through the center of the superconducting ring. The flux is defined by the surface integral:

$$\Phi = \int \vec{B} d\vec{S} \tag{2.2}$$

where $d\vec{S}$ is a vector perpendicular to the plane of the ring. Its length *dS* is an infinitesimal element of the area enclosed by the ring. But, by using the *Maxwell equation* (1.23) and *Stokes's theorem:*

$$\int (\nabla \times \vec{E}) d\vec{S} = \oint \vec{E} d\vec{l} \tag{2.3}$$

we can see that:

$$-\frac{d\Phi}{dt} = \oint \vec{E} d\vec{l} \tag{2.4}$$

where the line integral using dl is taken around the closed path at the edge of the ring. This path can be taken to be just inside the superconductor, and so $\vec{E} = 0$ everywhere along the path using the rotational symmetry of the loop. Therefore,

$$\frac{d\Phi}{dt} = 0 \tag{2.5}$$

and hence the magnetic flux through the ring stays constant as a function of time. We can use this property to set up a persistent current in a superconducting ring. First, we start with the superconductor at a temperature above T_C, so that it is in its normal state. Then apply an external magnetic field, B_{ext}. This passes easily through the superconductor since the system is normal. Now cool the system to below T_C. The flux in the ring is given by:

$$\Phi = \int \vec{B}_{ext} d\vec{S} \tag{2.6}$$

But we know from (2.5) that this remains constant, no matter what. Even if we turn off the source of external magnetic field, so that now $\vec{B}_{ext} = 0$, the flux Φ must remain constant. The only way the superconductor can keep Φ constant is to generate its own magnetic field $\vec{B}$ through the center of the ring, which it must achieve by having a circulating current, I, around the ring. The value of I will be exactly the one required to induce a magnetic flux equal to Φ inside the ring. Further, because Φ is constant the current I must also be constant. We therefore have set up a circulating persistent current in our superconducting ring. Furthermore, if there were any electrical resistance at all in the ring there would be energy dissipation and hence the current, I, would decay gradually over time. Different experiments observed persistent currents to remain constant over a period of years. In conclusion, the resistance must be exactly equal to zero to all intents and purposes.

2.3 The Meissner-Ochsenfeld Effect

Nowadays, the fact that the resistivity is zero, $\rho = 0$, is not taken as the true definition of superconductivity. The fundamental proof that superconductivity occurs in a given material is the demonstration of the *Meissner-Ochsenfeld effect* [25]. This effect is the fact that a superconductor expels the external magnetic field line from its material. First, consider the situation in which a small spherical sample of material is held at temperature T and placed in a small external magnetic field, $\vec{B}_{ext}$. Suppose initially we have the sample in its normal state, $T > T_C$, and the external field is zero. Imagine that we first cool to a temperature below T_C while keeping the field zero. Then later as we

gradually turn on the external field, the field inside the sample must remain zero. This is because, by the *Maxwell equation* (1.23) combined with $\vec{E} = 0$ we must have:

$$\frac{\partial \vec{B}}{\partial t} = 0 \tag{2.7}$$

at all points inside the superconductor. Thus, by applying the external field to the sample after it is already superconducting, we must arrive at the state where the magnetic field $\vec{B} = 0$ is zero everywhere inside the sample. But now consider doing things in another order. Suppose we take the sample above T_C and first turn on the external field, $\vec{B}_{ext}$. In this case the magnetic field will easily penetrate into the sample, $\vec{B} = \vec{B}_{ext}$. The *Meissner-Ochsenfeld effect* is the observation tha upon cooling the system below T_C, the magnetic field is completely expelled.

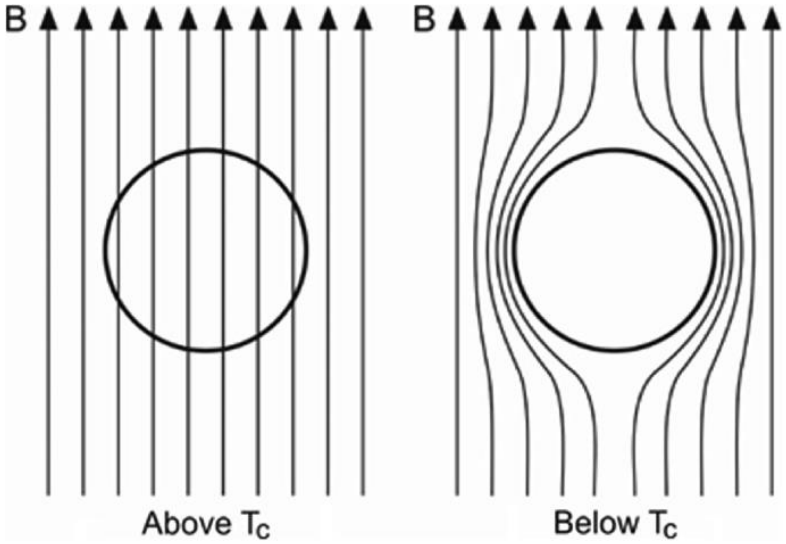

Figure 2.1: Superconductor expelling the magnetic field below the critical temperature.

This fact cannot be deduced from the simple fact of zero resistivity ($\rho = 0$) and so this is a new and separate physical phenomenon associated with superconductors. There are several reasons why the existence of the *Meissner-Ochsenfeld* effect in a sample is taken as definitive proof of superconductivity. At a practical level it is perhaps clearer to experimentally demonstrate the flux expulsion than zero resistivity, because, for example, it is not necessary to attach any electrical leads to the sample. A more fundamental reason is that the *Meissner-Ochsenfeld effect* is a property of thermal equilibrium, while resistivity is a non-equilibrium transport effect. In fact, one can see that we reach the same final state of the system when we first cool and then apply the field, or the other way around. Therefore, the final state of the system does not depend

on the history of the sample, which is a necessary condition for thermal equilibrium. It is perhaps possible to imagine exotic systems for which the resistivity vanishes, but for which there is no *Meissner-Ochsenfeld effect*. In fact, some *quantum Hall effect states* may possess this property [26]. Hence, we shall always define a superconductor as a system which exhibits the *Meissner-Ochsenfeld effect.*

2.4 Perfect Diamagnetism

In order to maintain $\vec{B} = 0$ inside the sample whatever (small) external fields are imposed as required by the *Meissner-Ochsenfeld effect* there obviously must be screening currents flowing around the edges of the sample. These produce a magnetic field which is equal and opposite to the applied external field, leaving zero field in total. The simplest way to describe these screening currents is to use *Maxwell's equations* in a magnetic. The total current is separated into the externally applied currents (for example in the coils producing the external field), $\vec{j}_{ext}$, and the internal screening currents, $\vec{j}_{int}$.

$$\vec{j} = \vec{j}_{ext} + \vec{j}_{int} \tag{2.8}$$

The screening currents produce a magnetization in the sample, M per unit volume, defined by:

$$\vec{\nabla} \times \vec{M} = \vec{j}_{int} \tag{2.9}$$

As in the theory of magnetic media, we also define a magnetic field H in terms of the external currents only:

$$\vec{\nabla} \times \vec{H} = \vec{j}_{ext} \tag{2.10}$$

The three vectors M and H and B are related by:

$$\vec{B} = \mu_0(\vec{H} + \vec{M}) \tag{2.11}$$

Maxwell's equations also tell us that:

$$\vec{\nabla} \cdot \vec{B} = 0 \tag{2.12}$$

The magnetic medium *Maxwell's equations* above are supplemented by boundary conditions at the sample surface. From (2.12) it follows that the component of $\vec{B}$ perpendicular to the surface must remain constant; while from the condition (2.10) one can prove that components of $\vec{H}$ parallel to the surface remain constant. The two boundary conditions are therefore,

$$\Delta\vec{B}_{\perp} = 0 \tag{2.13}$$

$$\Delta\vec{H}_{\parallel} = 0 \tag{2.14}$$

For simplicity we shall usually assume that the sample is an infinitely long solenoid. The external current flows in solenoid coils around the sample. In this case the field $\vec{H}$ is uniform inside the sample,

$$\vec{H} = I\frac{N}{L}\vec{e}_z \tag{2.15}$$

where I is the current flowing through the solenoid coil and there are N coil turns in length L. $\vec{e}_z$ is a unit vector along the solenoid axis. Imposing the *Meissner condition* $B = 0$ in (2.11) immediately leads to the magnetization:

$$\vec{M} = -\vec{H} \tag{2.16}$$

The magnetic susceptibility is defined by:

$$\chi = -\frac{dM}{dH}\Big|_{H=0} \tag{2.17}$$

and so, we find that for superconductors:

$$\chi = -1 \tag{2.18}$$

Solids with a negative value of χ are called diamagnets (in contrast positive χ is a paramagnet). Diamagnets screen out part of the external magnetic field, and so they become magnetized oppositely to the external field. In superconductors the external field is completely screened out. Therefore, we can say that superconductors are perfect diamagnets [27]. The best way to detect superconductivity in some unknown sample is therefore to measure its susceptibility. Thus, by measuring χ one will find $\chi = -1$ in a superconductor, evidence for perfect diamagnetism, or the *Meissner effect*. This is usually considered much more reliable evidence for superconductivity in a sample than zero resistance alone would be.

2.5 Type I and Type II Superconductivity

This susceptibility χ is defined in the limit of very weak external fields, $\vec{H}$. As the field becomes stronger it turns out that either one of two possible things can happen [28]. The first case, called a type I superconductor, is that the $\vec{B}$ field remains zero inside the superconductor until suddenly the superconductivity is destroyed. The field where

this happens is called the *critical field*, H_c. The magnetization obeys (2.16) for all external fields less than H_c, and then becomes zero (or very close to zero) for external fields above H_c.

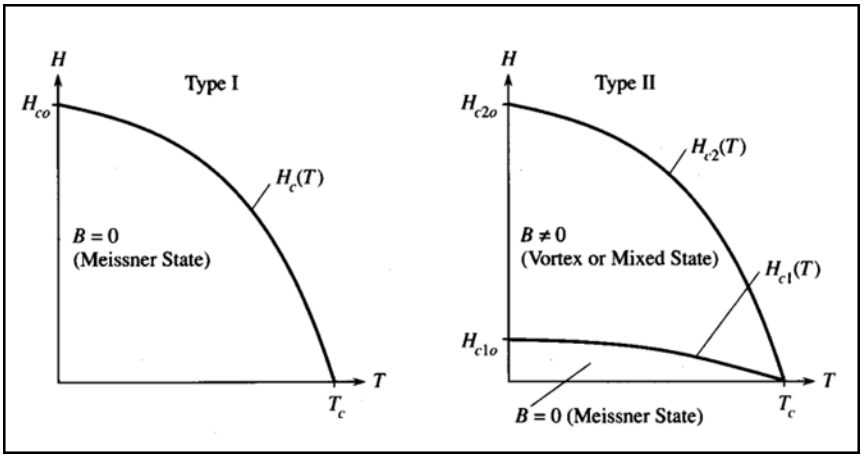

Figure 2.2: Type I and Type II superconductors [29].

In a type II superconductor, there are two different critical fields, denoted H_{c1}, the lower critical field, and H_{c2} the upper critical field. For small values of applied field $\vec{H}$ *the Meissner-Ochsenfeld effect* again leads to (2.16) and there is no magnetic flux density inside the sample, $B = 0$. However, in a type II superconductor once the field exceeds H_{c1}, magnetic flux does start to enter the superconductor and hence $B \neq 0$, and M is closer to zero than the full Meissner-Ochsenfeld value of $-H$. Upon increasing the field H further, the magnetic flux density gradually increases, until finally at H_{c2} the superconductivity is destroyed and $M = 0$. As a function of the temperature the critical fields vary, and they all approach zero at the critical temperature T_c. The physical explanation of the thermodynamic phase between H_{c1} and H_{c2} was given by Abrikosov [30]. He showed that the magnetic field can enter the superconductor in the form of vortices. Each vortex consists of a region of circulating supercurrent around a small central core which has essentially become normal metal. The magnetic field can pass through the sample inside the vortex cores, and the circulating currents screen out the magnetic field from the rest of the superconductor outside the vortex. It turns out that the magnetic flux inside a superconductor is quantized and each vortex carries a fixed unit of magnetic flux,

$$\Phi_0 = \frac{h}{2e} \tag{2.19}$$

and hence, if there are a total of N_v vortices in a sample of total area, A, then the average magnetic flux density, B, is:

$$B = \frac{N_v}{A}\frac{h}{2e} \tag{2.20}$$

2.6 The London Equation

The first theory which could account for the existence of the *Meissner-Ochsenfeld effect* was developed in 1935 by two brothers, F. London and H. London [31]. Their theory was originally inspired by the two-fluid model of superfluid ^4He. They assumed that some fraction of the conduction electrons in the solid become superfluid while the rest remain normal. They then assumed that the superconducting electrons could move without dissipation, while the normal electrons would continue to act as if the material had a finite resistivity. The superfluid electrons can be considered in parallel to the normal ones [32], creating a "short circuit" and making the overall resistivity equal to zero. We may denote the number density of superfluid electrons by n_s and the density of normal electrons by $n_n = n - n_s$, where n is the total density of electrons per unit volume.

Although this model is simple, several of its main predictions are indeed accurate. Most importantly it leads to the *London equation* which relates the electric current density inside a superconductor, $\vec{j}$, to the magnetic vector potential, $\vec{A}$, by:

$$\vec{j} = -\frac{n_s e^2}{m_e}\vec{A} \tag{2.21}$$

This is one of the most important equations describing superconductors. Nearly twenty years after it was originally introduced by the London brothers it was eventually derived from the full microscopic *quantum theory of superconductivity by Bardeen, Cooper and Schrieffer* [33].

Two important lengths can be found:

$$\lambda = \left(\frac{m_e}{\mu_0 n_s e^2}\right)^{1/2} \tag{2.22}$$

Where λ is the penetration depth of the superconductor, it is the distance inside the surface over which an external magnetic field is screened out to zero, given that $B = 0$ in the bulk.

$$\xi_0 = \frac{\hbar v_F}{\pi\Delta} \tag{2.23}$$

v_F the electron band velocity at the Fermi surface, and Δ the energy gap around the 0 frequency. The presence of an energy gap was observed shortly before the *Bardeen Cooper and Schrieffer (BCS) theory* was completed, and the energy gap was a central feature of the theory. ξ_0 is called the coherence length and it represents the physical size of the Cooper pair bound state in the *BCS theory*.

Considering l the mean free path of the electrons at the Fermi surface of the metal, the existence of the coherence length implies that a superconductor is characterized by no fewer than three different length scales. We have the penetration depth, λ, the coherence length, ξ_0, and the mean free path, l.

2.7 Thermal Fluctuations

Thermal fluctuations can make a very large contribution to the heat capacity, essentially diverging at the critical temperature T_c. Experimentally these thermal fluctuations are very difficult to see in standard pure superconductors, such as Pb or Nb. It is possible to estimate the range of temperatures near to T_c where these fluctuations are significant. This temperature range, T_G is known as the *Ginzburg criterion* [34]. In 1960 Ginzburg found that this temperature range is extremely small, i.e., much less than $1\mu K$ for most low T superconductors. Therefore, we can say that the original mean-field approach to *the Ginzburg Landau equations* [35] is perfectly well justified. However, in the high temperature superconductors, discovered in 1986, the coherence length ξ_0 is, very small of the order of just a few angstroms. It turns out that the corresponding Ginzburg temperature range, T_G, is of order of *1–2 K*. Hence, it is quite possible to see such thermal fluctuation effects in these systems. The specific heat near Tc clearly shows thermal critical fluctuations. Another example of thermal fluctuation effects can be seen in the resistivity, *ρ(T)*, just above T_c. Thermal fluctuations make *ρ(T)* begin to bend down towards zero even at temperatures quite far above T_c. This downward bending is clearly visible in the resistivity curve pf superconductors like of the $T_c = 135\ K$ superconductor $HgBa_2Ca_2Cu_3O_8 + \delta$ [36].

2.8 Vortex Matter

Another very important consequence of thermal fluctuations occurs in the mixed state of high temperature superconductors. *Abrikosov's flux lattice theory* [30] shows that the vortices align in a periodic lattice arrangement, essentially like a crystal lattice, either triangular or square. However, this is again a mean field approximation. We must, in principle, again include the effects of thermal fluctuations.

The theories of the resulting vortex matter states show a very wide range of possibilities. It is still possible to talk about the vortices, but now they themselves form

a variety of different states, including liquid and glassy states, as well as nearly perfectly ordered crystalline states. It is believed that the flux lattice never has true crystalline order, and thermal fluctuations always lead to an eventual loss of long ranged order in the periodic structure.

Unfortunately, these thermal fluctuations are undesired for commercial applications of high T_c superconductors in high current wires and electromagnets. The problem is that thermal fluctuations lead to motion of the vortices, and this leads to a source of energy dissipation. Therefore, the resistivity is not zero for high T_c superconductors in a magnetic field. The problem also occurs in low T_c superconductors, but to a much lesser extent. In these systems the energy dissipation due to the motion of vortices can be reduced or eliminated by providing pinning centers which "pin" the vortex lattice and prevent it from moving. Typically, these are just impurities, or naturally occurring crystal defects such as grain boundaries and dislocations [21].

To see why motion of vortices leads to energy dissipation is necessary to see that a current density $\vec{j}$ flowing through the vortex lattice (perpendicular to the magnetic field) leads to a Lorentz force on each vortex. The overall force is:

$$\vec{f} = \vec{j} \times \vec{B} \tag{2.24}$$

per unit volume of the vortex lattice. This will tend to make the vortex liquid flow in the direction perpendicular to the current. If the vortices flow in response to this force, work is done and there is energy dissipation. To calculate the work, consider a loop of superconducting wire, with a current flowing around the wire. Vortices will tend to drift transversely across the wire, say entering on the inner side of the wire and drifting over to the outer side. Each vortex carries a magnetic flux Φ_0, and so the total magnetic flux in the ring Φ changes by Φ_0 with each vortex that crosses from one side of the wire to the other. But there is an electromagnetic field induced in the wire given by (2.4). Power is dissipated, at a rate given by $P = VI$, where I is the total current. Hence, vortex motion directly leads to finite resistance. In the mixed state and stead state operation, superconductors only have truly zero resistance when the vortices are pinned and unable to move [37].

In high T_c superconductors the thermal motion of vortices leads to especially bad pinning and hence a significant resistivity in the mixed state. To make matters worse, the lower critical field H_{c1} is tiny, often less than the Earth's magnetic field, and so vortices can never be truly eliminated. At high temperatures and near to H_{c1} it is believed that the vortex matter is in a liquid state, and so the vortices can move freely and pinning is essentially impossible. Lowering the temperature or going further away from H_{c2}, the vortex matter appears to "freeze" into a glassy state. A glass is random spatially, but frozen in time. Since glass is effectively rigid the vortices cannot move

and pinning is able to largely prevent flux motion, so in this state the resistivity is quite low. Unfortunately, even in this glassy vortex state the resistivity is not fully zero, since flux creep can occur.

The random pinning force provides a set of energy barriers to vortex motion. However, due to thermal motions, from time to time, the vortices can hop over the local energy barrier and find a new configuration. The line in the *(H, T)* phase diagram where the glassy phase occurs is called the *irreversibility line*. Something approaching zero resistivity is approached only well below this line. This effectively limits the useful magnetic fields for applications of high T_c superconductivity, to very much less than the hundreds of Tesla that one might have expected from the nominal values [38].

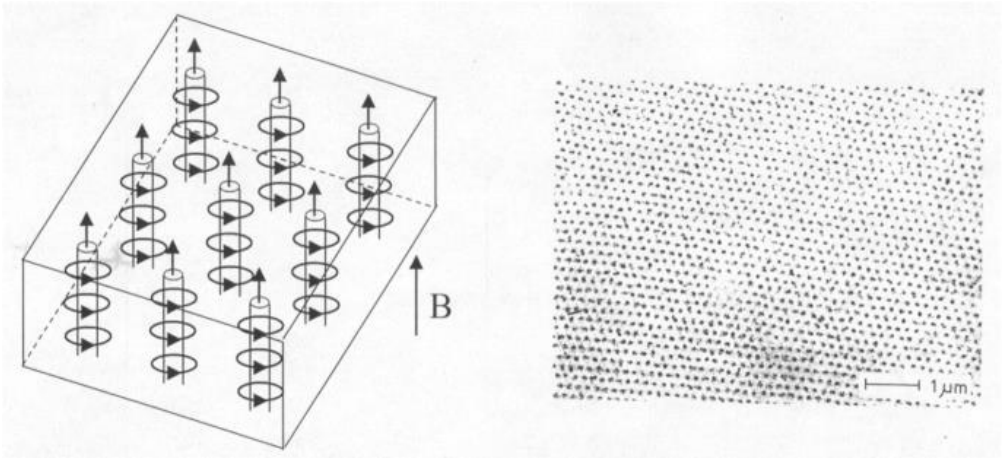

Figure 2.3: Vortexes in superconductors [30].

2.9 MgB_2

MgB_2, a well-known material with superconductive properties, has already found several industrial applications, such as in magnetic resonance imaging. Its widespread use and the availability of existing models and data make it suitable material for this master thesis.

The discovery of MgB_2's superconductivity in 2001 [39] opened up possibilities for the development of high-temperature superconducting materials that do not require extremely low temperatures, like liquid helium cooling. MgB_2 offers several advantages over other high-temperature superconductors. It allows current flow without barriers between grain boundaries, making it feasible to work with polycrystalline material instead of expensive single crystals. MgB_2 is also abundant, cost-effective, easy to manufacture, and has low density and excellent mechanical properties.

MgB_2 is classified as a type II superconductor. Below its transition temperature ($T_C = 39\ K$), it exhibits perfect diamagnetism up to a critical field value (H_{c1}). In the range of $H_{c1} < H < H_{c2}$, the material allows the penetration of magnetic fields through quantized flux lines. However, beyond H_{c2}, superconductivity is lost. In this intermediate field regime, the flux lines or vortices experience Lorentz forces, causing lateral displacements that result in energy dissipation and hinder the complete realization of the superconducting state. Therefore, the introduction of pinning centers through doping becomes necessary to immobilize the flux lines and prevent energy dissipation during the passage of supercurrents.

To better understand MgB_2's properties and optimize its functionality, it is essential to analyze its crystal structure. MgB_2 consists of alternating layers of boron and magnesium arranged in a hexagonal lattice along the c-axis. The boron atoms form a honeycomb arrangement similar to graphite, with each atom equidistant from three others. The magnesium atoms are located at the centers of cavities defined by boron hexagons. The crystal structure of MgB_2 is depicted in Figure 2.4.

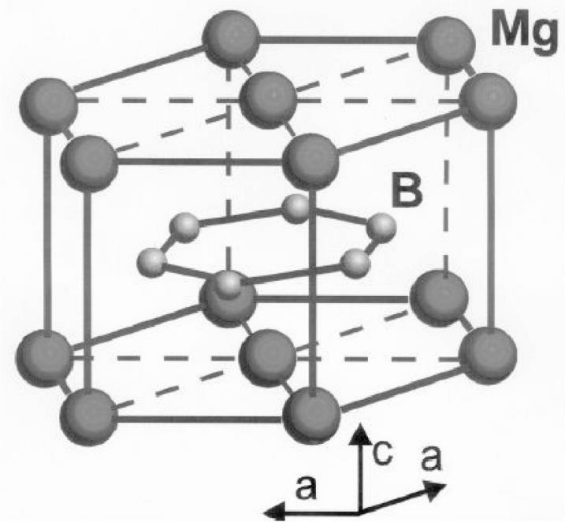

Figure 2.4: Crystalline structure of MgB_2 [40].

The presence of boron, particularly in its layered structure, is believed to be a crucial factor in achieving "high temperature" supercurrent in MgB_2. The pronounced structural anisotropy of MgB_2 is evident even at varying temperatures. Studies have shown that the coefficient of thermal expansion along the c-axis is twice that along the a-axis. Similar behavior has been observed in compressibility measurements at constant temperature [41]. Theoretical calculations reveal that as the temperature decreases, the strong covalent bonds between boron atoms are maintained, while the magnesium atoms tend to ionize and transfer valence electrons to the conduction band derived from the boron lattice [42], similar to the simplified structural analogy with

graphite. Therefore, the superconductivity of MgB_2 is primarily attributed to the metallic nature of the two-dimensional sub-lattice structure of boron, which is characterized by high vibrational frequencies and a Debye temperature of 920 K [43], contributing to its observed high value of T_C.

In its ideal crystal form, pure and free from extended lattice defects, MgB_2 can only be used at magnetic fields below 3 T (typically at a temperature of 20 K). In comparison, the currently available superconducting material, $NbTi$, can withstand fields up to 7 T (when maintained at 4.2 K). Consequently, it is possible to effectively utilize MgB_2 doping the crystal with carbon and increase its critical current in the presence of high magnetic fields, which are desirable operating conditions for superconducting materials. Therefore, the use of doped MgB_2 is convenient for technological and industrial reasons, for these motives it was chosen as superconducting material in the coils.

3. Goals and Components

3.1 Aim of the thesis study

The goal of this analysis is to make a preliminary design of a superconducting dipole magnet, substituting an already existing normal resistive magnet. In the thesis different steps that will be fulfilled will be to make some considerations over the dimensions, workload, materials and design choices to lower the power consumption and obtain new information on low field dry superconducting magnets. It was considered principally MgB_2 has coils component due to its high versatility, low cost and availability. Moreover, ASG Superconductors is one of the leading leaders in MgB_2 superconductor production, hence is a well-studied material with year of practical applications.

As previously mentioned, it was considered the magnetic resistive dipole nowadays working at CNAO, Pavia, Italy. The CNAO synchrotron, because of the beam current limitations from the injector, was not designed to be operated in the MEE mode (multi-energy extraction): its magnets are ramped-up and down for each of the energy values required by the treatment plan. The ramp up and ramp down time are 10 s long with a maximum magnetic field in the bore of $1.8 - 2\ T$. The presence of this high variation in time has a great impact on the final design, the power consumed by a superconducting magnet during a steady state is virtually 0 [2], instead with time varying magnetic there is an high-power consumption of the AC losses and the possible presence of eddy currents, see section 1.4.2, on the thermal shield. However, an analogous study could be performed on any superconducting magnet adjusting the hypothesis and boundaries conditions, for example one of the other projects carried on by INFN-LASA study the possibility to upgrade in a similar way the PSI magnet, which works in steady state mode. The current magnet at CNAO is a 5-meter-long dipole, composed of an iron yoke and a copper coil. It is water cooled with an averaged power consumption over a year of 30 kW. The Dipolar «Window-Frame» Bending Magnet, Figure 3.1, is bended downward and the two coils are symmetrical with a

saddle shape. It is important to consider that the two "faces" (on the left and on the right) of the magnet have a different angle, 30° and 21° respectively, to exploit field edge effects on the particles to be accelerated.

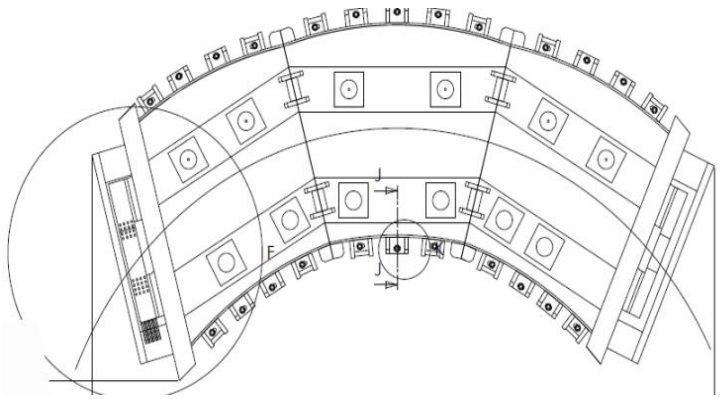

Figure 3.1: CNAO dipole magnet.

It was decided to keep the iron yoke without modifications and substitute the copper coil with MgB_2 rope windings [44]. The section of the copper coil is 398 mm x 114 mm. The superconducting ropes will occupy less space than the copper ones, so that the cryogenic system can be fitted in the remaining space inside the yoke. As can be seen from the Figure 3.2 the void gap is very narrow on the vertical axis and broad on the horizontal one, hence a classical cryogenic liquid bath is an expensive and not fully optimized design.

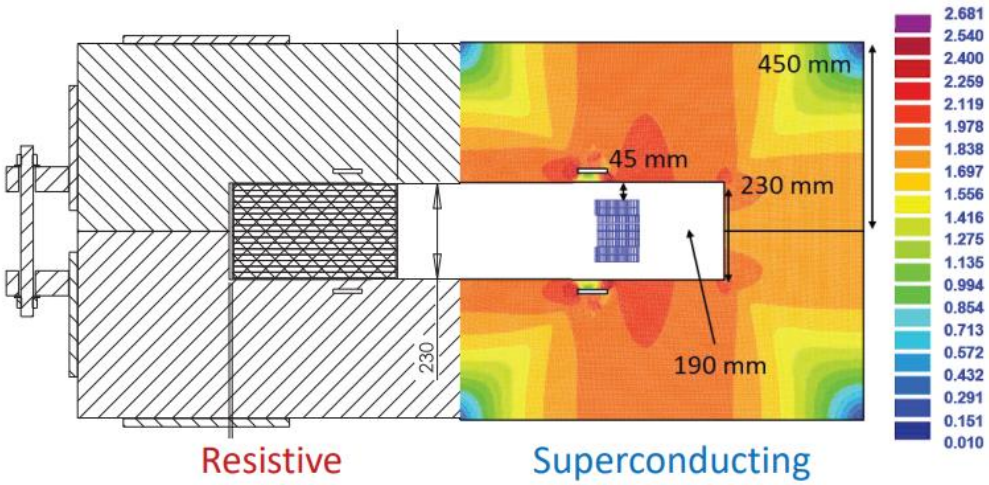

Figure 3.2: Frontal section of the normal resistive magnet (left side) and modelling of the superconducting coils with magnetic field map (right side).

Moreover, MgB_2 has a critical temperature of ~39 K hence it must be cooled by liquid helium or has to be placed inside a vacuum chamber connected to one or more cryocoolers. Due to the high market price of the liquid helium and the quite large dimensions of the magnet, it was decided to place the coils inside a vacuum chamber and cool it through several cryocoolers by direct contact. The vacuum chamber is used to minimize heat transfer from the iron yoke to the coils and the cryocoolers exploit the high thermal conductivity of the coils and thermal shield materials to remove the heat arriving on the coils and generated by them.

To avoid high energy deposition on the coil, due to the high temperature difference with the ambient temperature of the yoke, a thermal shield was placed between the coil and the yoke. It is important to remember that the heat is mostly radiative hence by the *Stefan–Boltzmann law*, it will highly depend on T^4 of the hottest face and on the emissivity of the materials (at cryogenic temperature the used materials will have an emissivity approximately equal to 0.3). Supposing to work with the coils at 10 K, the presence of an intermediate stage at a lower temperature (60 K) will lower sensitively the heat arriving on the coils. Lastly, to avoid direct contact, and hence conduction, between the components at different T it was decided to keep the coil and thermal shield suspended, they are anchored to tie-rods, hence thermal conduction will be localized in small areas. The tie-rods will also support the magnet and give it stability against the Lorentz forces generated during the operations. Other cooling components were considered such as multi-layer insulator. It is important to notice that in a superconducting system the most critical component is the superconductor itself due to its temperature constrains, so it will be very important to have a satisfactory temperature margin and avoid an excessively thermal increase during operations.

Once defined the goal, it was decided to analyze separately the effect on each possible configuration on the temperature profile of the coil, the current leads power consumption and the coils to focus on the effect that each component has on the temperature profile and power consumption of the magnet. As stated above, the main focus will be the coils' temperature profile and behavior to avoid any possible accident and to maximize the superconductor.

3.2 Coils

To have the required field in the bore the superconducting coil is divided in 4 blocks, as shown in Figure 3.3(a). The position of the blocks of the upper coil is symmetrical

within respect to the lower one and the same can be said for the right and left parts of the coil.

Each block will be made of several superconducting ropes, the total number can be varied keeping the total current constant, but the effect of the different number of the ropes will be analyzed subsequently, section 4.2.4.

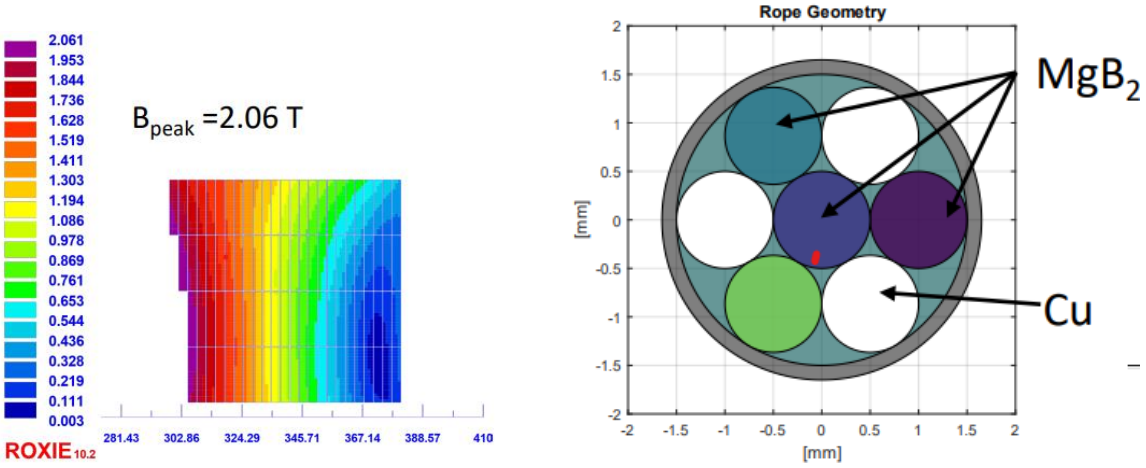

(a) Coil modelling (b) Superconducting rope composition

Figure 3.3: Coil composition.

For the first analysis we will consider 1260 total ropes divided equally for each coil. Each rope will be composed as in Figure 3.3 (b), it will contain 3 MgB_2 wires and 4 copper ones, each with a radius of 1 mm. They will be insulated with S2-glass fiber for a total rope diameter of 3.3 mm. Finally, the rope is impregnated with epoxy resin matrix to compose the blocks. For sake of simplicity the material properties of epoxy resin will be taken both for the insulation layer and the impregnated matric.

For a further simplification the cross-section of the coils is considered rectangular and homogeneously composed, with dimensions and ropes compositions as in the Table 3.1.

	width coil	**height coil**	**rope radius**	**thick. resin**	**length**
[m]	0.1056	0.1473	0.0015	0.00015	5
	$\boldsymbol{MgB_2}$	$\boldsymbol{Cu}$	$\boldsymbol{Ni}$	$\boldsymbol{Nb}$	$\boldsymbol{Monel}$
%	11.5	14	14	14.5	46

Table 3.1: Coil simplified dimensions and composition of the rope.

3.3 Thermal Shield

As said at the beginning of this chapter, to reduce the heat load on the coils is convenient to add a thermal shield inside the vacuum chamber. Due to the length of the magnet, it is very important to use a material with high thermal conductivity at low temperatures. This will help to keep the hottest point in the thermal shield as low as possible to lower thermal transfer to the coils.

The materials chosen for this analysis are copper and aluminum, both have a thermal conductivity one order of magnitude higher than the stainless steel one. It is remarkable that these two metals have a relatively low density compared to other metals, hence the thermal shield will have a lower weight and will weigh less on the tie rods, although the principal forces on the tie-rods will be the Lorentz ones.

Another effect to consider is the presence of induced eddy currents during the ramp up and ramp down of the magnetic field. Due to the high field gradient, the currents can be significantly high leading to heating caused by the *Joule's Effect*. To avoid this currents, ASG Superconductors designed a thermal shield having copper or aluminum slabs divided on two alternate layers connected by epoxy resin, this will reduce to almost to zero the longitudinal electrical conductivity without lowering noticeably the transversal thermal conductivity or the mechanical strength of the shield.

To have a clear picture of the thermal transfer inside the magnet it is important to analyze the temperature in the thermal shield at the furthest point from the cryocoolers and the thickens of the shield. This last characteristic will mostly depend on the available standards and their prices without affecting much the whole thermal analysis. Moreover, the distance of the thermal shield form the coils is very important as we will see in the analysis.

3.4 Multi-layer Insulation

Due to the dimensions of the magnets the surface of the thermal shield is high, so it will be very important the radiative contribution in the thermal balance. A way to limit the radiative power is the use of MLI or Multi-layer insulation, it is a thermal insulation composed of multiple layers of thin sheets of aluminized mylar. It is primarily intended to reduce heat loss by thermal radiation. In its basic form, it does not appreciably insulate against other thermal losses such as heat conduction or convection.

All the objects will radiate energy, how much of that energy radiates it depends on the emittance ε of that object's surface. High emittance means that the object will cool faster by radiation, if the surroundings are cold. Low emittance means that the object

will stay warm longer, even if the environment is cool. Another quantity is α, the absorptivity. High α means that the object will heat faster by radiation. The factors ε and α are the difference between black body radiation, and *"grey body radiation*". These factors just account for the fact that not all surfaces are black, meaning that some surfaces reflect light. A body with high a high ratio of α/ε will get very hot under radiation, even if both values are very low.

As a side note, absorptivity + reflectivity + transmittance = 1, this means that all light gets either absorbed, or reflected or let through a surface.

Usually, it would be preferred to use materials that are transparent to the radiation and highly emitting in the infrared as a cover (substrate). This is often brownish Kapton. Below that there will be a material that reflects as much of the energy as possible, which usually is silver or aluminum.

The principle previously described is applied to the outer layers of the insulator. The internal structure of a multi-layer insulator is composed of multiple reflective layers, each one composed of a plastic substrate in mylar with a reflective metal coating in aluminum on both sides. Such layers are distanced with spotted spacers or a Dacron web to reduce as much as possible the conduction heat transfer.

In this analysis, to lower the cost, were chosen commercially available MLI. It is possible to buy them in sheets of 10 layers with thickens of 3.5 mm. To avoid conduction and hence degradation of the MLI utility, we will analyze if there is enough space for the MLI on the thermal shield surface and on the coils, analyzing if it has a positive and sensible effect on the thermal analysis and how many layers is more convenient to work with.

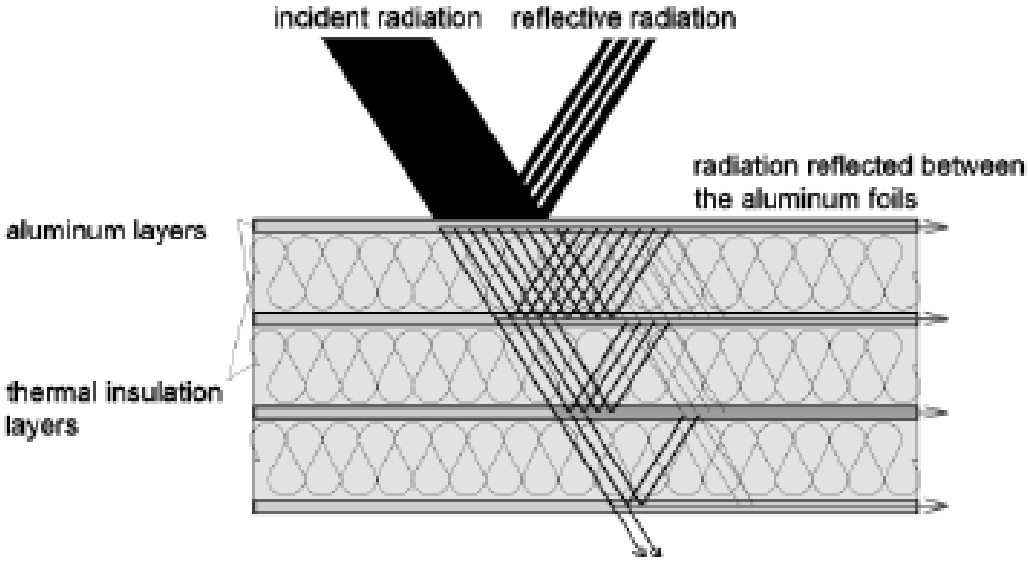

Figure 3.4: Functioning of MLI [45].

3.5 Tie-Rods

As previously mentioned, it is important to reduce as much as possible the surface that leads by conduction the heat from the yoke to the coils limiting the thermal load on it. To do so the coils are kept suspended through tie rods. They are not only important on the thermal side but have also the function of keeping the coils position fixed to avoid stability problems on the beam line and they must contain and support the two coils. Notice that also the thermal shield is connected to the tie-rods.

So, it is necessary to find a material with low thermal conductivity at cryogenic temperature and, most importantly, a material with high mechanical strength. In this analysis this goal is achieved by G10, a glass fiber soaked with epoxy resin, as the resin has a very low thermal conductance but has a high yield strength at low temperature, several times higher than stainless steel. The tie-rods must have a small as possible transversal surface to lower heat transfer and must withstand a radial Lorentz force of 14.2 $^{Kg}/_{m}$ in addition to the weight of the coils and the thermal shield-.

As explained above, a small surface is required hence the rods will have a ratio, length to section diameter, very high. Due to the outward radial nature of the Lorentz's force on the coils, the rods will be subjected to compression and so they could fail due to buckling (Section 1.3.3). To avoid this situation, the tie-rods are pre-loaded (elongated) and so they will work in tension even under the influence of the force of the coils.

Another possible design for the support that was not considered in the analysis is the possibility to use hollow cylinders instead of tie-rods to have an equally small area but a more spatially distributed heat conduction. However, the use of cylinders will require a specific design and construction while the tie-rods are already industrially produced and hence right away available and at a lower cost.

3.6 Cryocoolers

Cryocoolers are fundamental to allow the system to work at cryogenic temperature, and the choice of which model utilize depends on the thermal conditions of the magnet. In this analysis it was decided to work with pulse tube cryocoolers (PTC). They were chosen due to their two-stage nature, hence it is possible to connect the hot head of the PTC to the thermal shield and the cold one on the coils minimizing the number of cryocoolers utilized and hence lowering construction and operational costs.

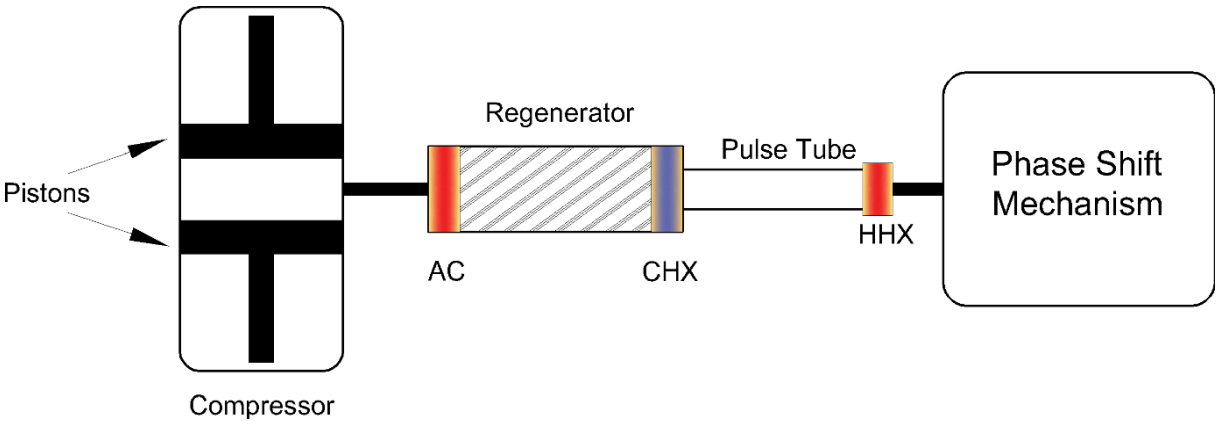

Figure 3.5: Pulse tube cryocooler schematics [46].

They rely on the theory of oscillatory compression and expansion of an ideal gas within a closed volume to achieve the desired refrigeration. PTCs, like other regenerative cryocoolers, utilize the compression/expansion of working gas to remove heat. The main merit over other types of cryocoolers, like Stirling and Gifford–McMahon machines, is that PTCs do not need a mechanical displacer or even a motorized valve mechanism to guarantee that a phase shift is set between the pressure signal, provided by the compressor, and the volumetric flow rate in the tube.

Conventional PTCs are composed of a few key parts as depicted in Fig. 3.4. The compressor is conventionally either of reciprocating or dual opposed piston type, with linearly moving magnets, its main function being to deliver an alternating pressure via controlling the electrical drive on the magnets. The regenerator is the most vital part in any PTC, characterized by its efficiency. It is generally of porous nature, conventionally containing stacked mesh screens and/or spherical particles with high heat capacity and low thermal conductivity, with the function of receiving heat during the pressurization phase and delivering it back to the returning gas during depressurization. Clearly an ideal regenerator should not store thermal energy after one cycle.

The aftercooler (AC) is introduced to pre-cool the incoming gas from the compressor, reducing the temperature at the hot end (HHX) and causing the regenerator to supply low temperature gas more efficiently. Continuous water or air cooling is required at both the hot end heat exchanger (HHX) and the aftercooler to pick up any generated heat, and thus maintaining these positions at room temperature. The cold end (CHX) acts like the evaporator in a classic vapor–compression refrigeration cycle and is the position where a target object is to be mounted.

Along with the regenerator, the pulse tube is also a crucial element for correct PTC operation. Its main function is to reject heat, through enthalpy flow, from the cold end

to the hot end due to the presence of a phase shift mechanism. Conventionally, the pulse tube is a hollow tube made of stainless steel, with minimal thickness to reduce radial heat transfer, and optimized to provide a uniform temperature gradient along the tube between the cold and hot ends.

Phase shift mechanisms are essential to produce a significant cooling effect. The aim is to provide a phase shift, within the periodic cycle, between the source pressure signal and the resultant volumetric flow rate. The phase difference results in a steady temperature variation across the pulse tube. Conventionally, this has been achieved by introducing extra components including an orifice opening, an inertance tube, a buffer volume (reservoir), and/or a second bypass orifice after the hot end of the PTC system.

In this model will be utilized cryocoolers with the hot head connected to the thermal shield at 77 K and the cold one connected to the coils at 10 K. The choice of which model to choose depends on the power extracted from the heads, most importantly the cold one. The models considered will come from Cryomech, leading company in the sector [47]. As previously mentioned, it is necessary to cool the regenerator, hence water chilled will be used [48].

Several combinations of positioning and total number of cryocoolers are considered to have a clear knowledge of the thermal condition in each design.

3.7 Current Leads

The powering of a superconducting system requires transfer of current from ambient temperature, where the current is generated, to the cryogenic environment. This electrical transmission, which takes place inside a cryostat, is performed by the current leads, devices that transport current in a significant gradient of temperature and represent, therefore, one of the major sources of heat inlet into the cryostat.

Good electrical conductors are also good thermal conductors, and the transfer of electrical current in metals that operate in a gradient of temperature, for which one needs to minimize both ohmic losses and thermal conduction, is bound by the existence of a minimum heat inlet into the cryogenic environment.

For the heat losses in the hot head of the cryocoolers will be considered brass current leads. Instead, in the cold section brass current leads are compared to HTS current leads while the former will have a fixed power dissipation.

4. Model and Data Analysis

In the following chapter it will be analyzed the model created to make a preliminary estimate of the energy saved by substituting the normal conducting magnet with a superconducting one, with results referring to the CNAO facility (PV) [2]. The main goal is to reduce the power consumed annually by the magnet of a gain factor equal to $5 \div 10$. Introducing a significative energy saving can boost the utilize of the accelerator, and in the near future increase its medical use.

4.1 Input parameters

The model needs different input parameters to work correctly. Their values change for each magnet considered and for some of them a preliminary analysis is required.

First, the temperature boundary conditions are required, the model requires the temperatures fixed by the cryocoolers, hence the temperature of the thermal shield and coils ends and at these two data it is added the external temperature of the iron yoke (usually the ambient temperature).

In this project, since the iron yoke is kept unchanged to shape the magnetic field in the bore, after a field analysis the coils dimension is found and optimized. Accordingly, the internal and external dimensions of the chamber are given. Alongside the magnet length the four transversal dimension parameters are needed to compute the heat transfer from the yoke to the coils.

For the coils we need the rope dimensioning and their composition, thus the rope radius, the thickness of the insulator and the percentage of each element constituting each rope are required.

Lastly, there are several parameters given by other preliminary analysis:

- thickness of the thermal shield;
- material of the thermal shield;
- internal gap dimension;
- total number of the ropes;

- Lorentz force on the coils;
- yielding strength of the tie-rods material;
- number of the tie-rods per meter;
- number of the cooling sides, or the number of the coolers utilized;
- number of layers of MLI on the thermal shield and on the coil;
- AC losses.

4.1.1 Initial conditions

	T coil	**T shield**	**T yoke**
[K]	10	60	300

Table 4.1: Boundary temperatures.

	width coil	**width yoke**	**height coil**	**height yoke**	**length**
[m]	0.1056	0.44	0.1473	0.228	5
	thick. shield	**internal gap**	**rope radius**	**thick. resin**	
[m]	0.005	0.01	0.0015	0.00015	
	$\boldsymbol{MgB_2}$	$\boldsymbol{Cu}$	$\boldsymbol{Ni}$	$\boldsymbol{Nb}$	$\boldsymbol{Monel}$
%	11.5	14	14	14.5	46

Table 4.2: Dimensions and material percentage inside the ropes [2].

	Lorentz force	**yielding**	**number tie-rod**	**power losses**
various	142000 [N/m]	$3.447 * 10^8$[Pa]	2.2 [1/m]	4 [W/m]
	MLI coil	**MLI shield**	**cooling sides**	**ropes**
quantity	20	30	2	2560

Table 4.3: Preliminary considerations.

4.2 Model

The model created for the analysis of the problem can be divided in three main sub-models:

A thermal one, in which is analyzed the total power extracted in steady state regime, with focus on the coil power and its temperature profile.

A sub-model will focus on the current leads' behavior, considering resistive leads and superconducting ones.

Finally, the last one will consider the coil's parameters analyzing the change in power losses, the safety margin and the number maximum of duty cycle before reaching the critical temperature.

4.2.1 Hypothesis

To simplify the model without compromise the results, several assumptions were made:

Hypothesis 1: The magnet is considered horizontal and straight while actually it is bended downward.

Hypothesis 2: One dimensional heat transfer is considered, in particular the heat transfer of the coils is uniform along its whole surface.

Hypothesis 3: Thermal radiation load is obtained utilizing the smallest gap present between the two transversal dimensions.

Hypothesis 4: The thermal shield will be considered without transversal temperature change, the inner face and the outer one will have the same temperature profile.

Hypothesis 5: Coil material is considered homogeneous; the properties are isotropic.

Hypothesis 6: The area for the transversal heat flux is always chosen as larger as possible to be more conservative.

Hypothesis 7: No radiative longitudinal heat on the coil is considered, its negligible.

Hypothesis 8: Power loss in the coil during the transient is only caused by hysteresis, because is far higher than the inter filament and intra filament contributions.

Hypothesis 7: During the duty cycle the cryocoolers won't keep up with the coil, hence there will be an adiabatic heating.

Hypothesis 8: The two magnetic coils' sections are considered as a unique rectangular piece, hence will contain more resin matrix and will worsen thermal conductivity.

Hypothesis 9: The thermal shield surrounds completely each side of the coils, this is not real, in the bore-side there isn't the shield. Moreover, there will be only one thermal shield enclosing both sides. This consideration will only increase a bit the total heat flux without changing much the results.

Hypothesis 10: The heat flux on the coils is uniform, neglecting the hot spot due to the tie-rods.

4.2.2 Thermal model of the magnet

This model will analyze the thermal transfer and temperature profile of the system, obtaining several geometrical considerations alongside the total power extracted in the thermal shield and in the coils by the cryocoolers. Different configurations are considered, the main goal is to minimize the energy extracted considering the lowest thermal load possible on the coils.

To start a rectangular shape coil is analyzed, enclosed by a thermal shield and sustained by the tie-rods, which are connected to the internal surface of the iron yoke (Hypothesis 8 & 9).

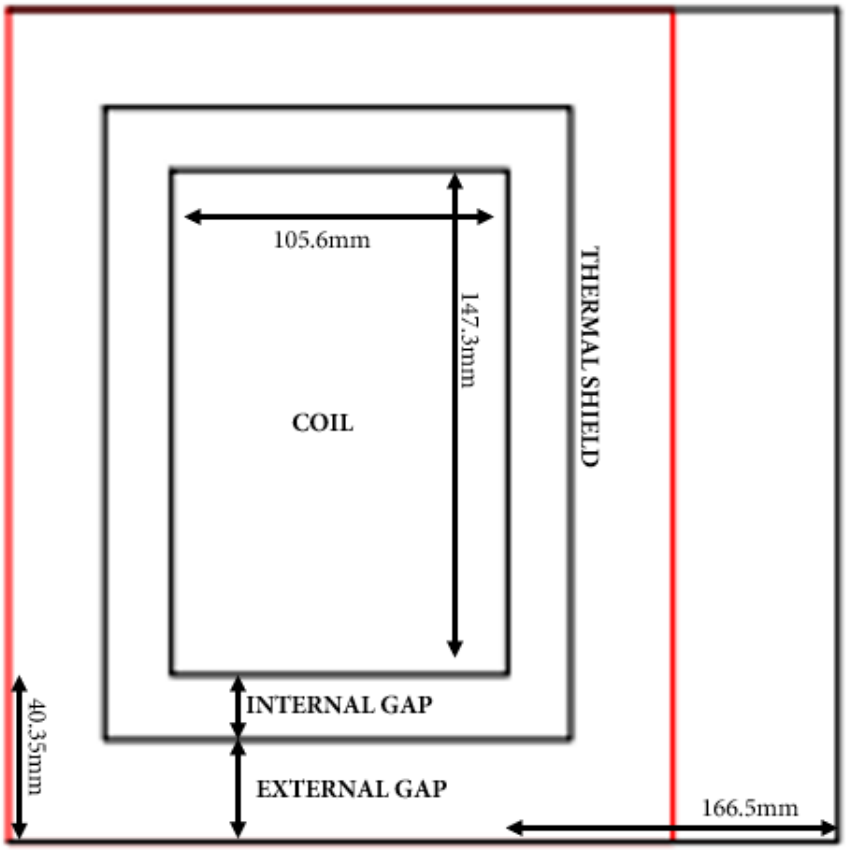

Figure 4.1: Schematical section of internal part of the magnet

In the Figure 4.1 the real yoke shape is depicted in black, instead the reduced configuration with a smaller area is depicted in red. In the model will be mostly used the reduced area.

Dimension of the gaps

The dimension of the two gaps and the thickness of the thermal shield heavily influences the thermal transfer problem of the system.

Firstly, it was decided to use a thermal shield 5 mm thick. It was fixed at that value to keep Hypothesis 4 true, and this is a value of commercially available slabs of several materials, such as aluminum and copper.

Once decided the thermal shield thickness and the spacing between the coils and the yoke, the value of the two gaps' thickness are connected, hence in analysis it will be considered mainly the internal one.

In addition to the relation between the two linear power density and the internal gap, it was also considered the use of the MLI when the spacing allows its presence, depending on how many layers are used. To evaluate the radiative heat transfer of the MLI exist several models, it was chosen a model used at CERN that fits the MLI utilized [49].

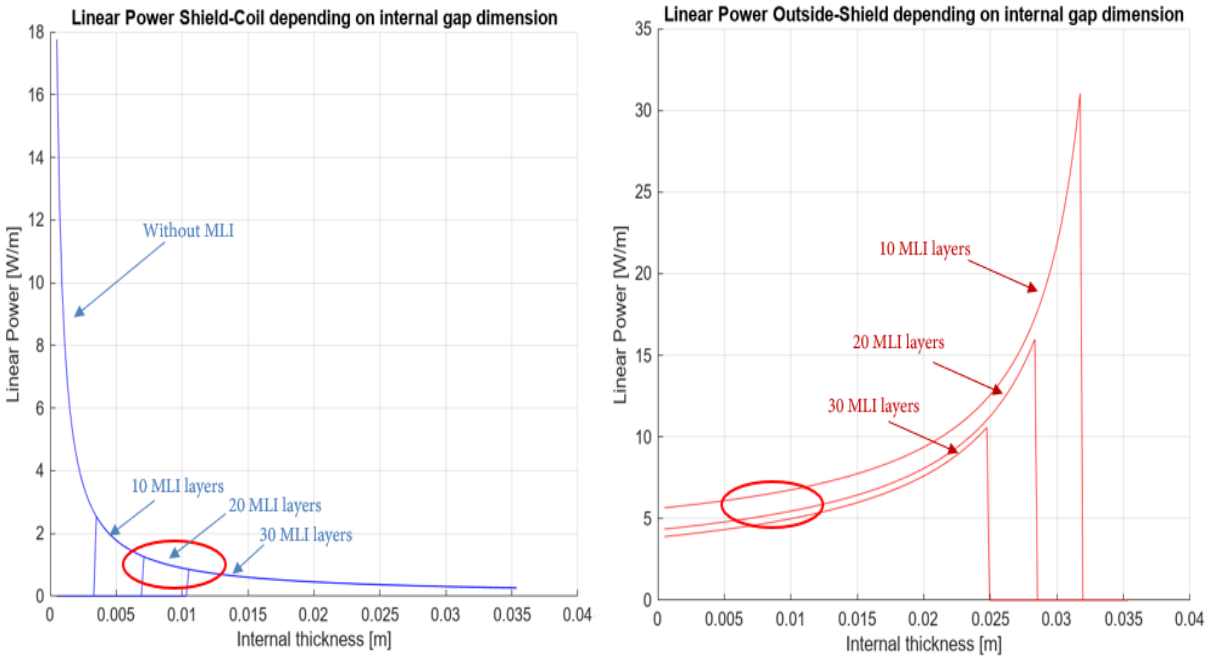

Figure 4.2: Dependence on the internal gap dimension of the linear power density from the shield to the coil (left) and from the yoke to the shield (right).

To minimize the linear power density arriving on the thermal shield and on the coils, it was selected an internal gap thickness of 10 mm. Moreover, it was decided to utilize 20 layers of MLI in the internal gap and 30 in the external one, to lower the power density and to avoid possible contact between the shield and the boundaries if any oscillation occurs.

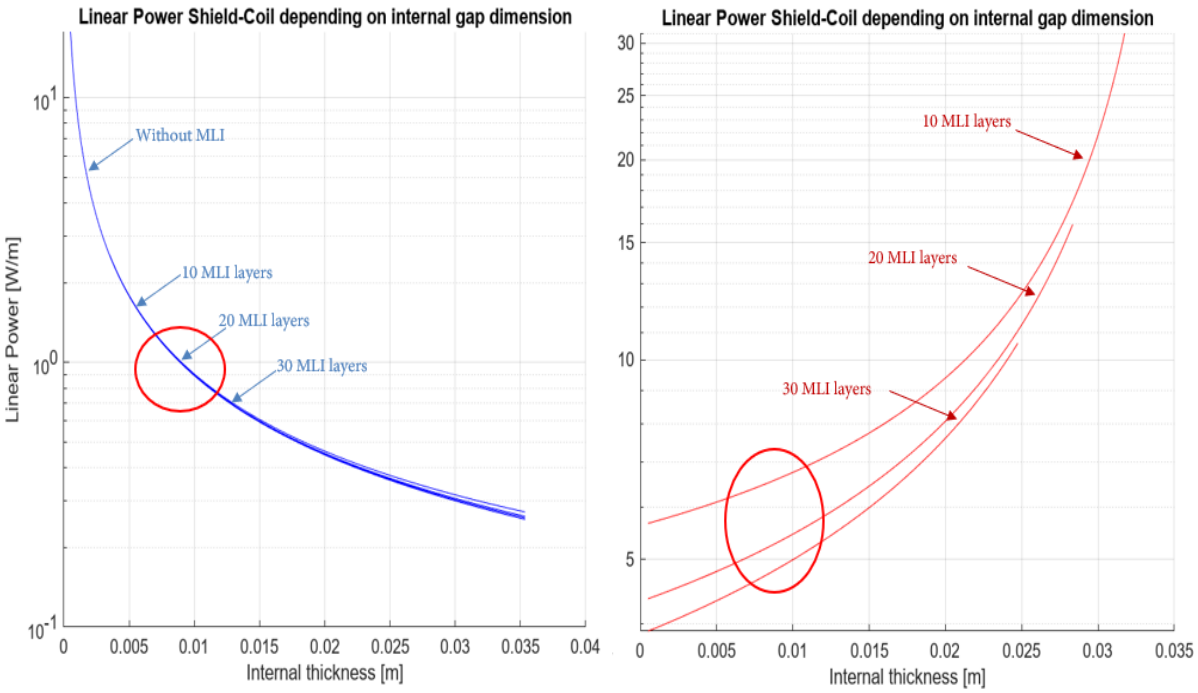

Figure 4.3: Dependence on the internal gap dimension of the linear power density in logarithmic scale from the shield to the coil (left) and from the yoke to the shield (right).

Tie-rods

The choice of how many tie-rods utilize and which configuration set up is very important in the thermal analysis of the system because thermal conduction of the tie-rods is the main component of the heat transfer.

First, it is important to decide how many tie-rods utilize, hence what is their diameter. Industrially are produced G10 rods with an integer radius so only tie-rods with an even diameter will be considered. Depending on the number of tie-rods per meter and knowing the Lorentz force per meter, mass of the coil and the thermal shield, the surface of the rods is obtained following:

$$S = \frac{F_L + g(m_{shield} + m_{coils})}{\sigma_{tir} \cdot N_{tir}} \tag{4.1}$$

Where F_L is the maximum Lorentz force acting on the coils, g the gravitational constant, m_{shield} the mass of the thermal shield, m_{coils} the mass of the coils, N_{tir} the total number of tie-rods and σ_{tir} the stress value obtaining applying the TRESCA criterion [50] to the yielding stress of the G10.

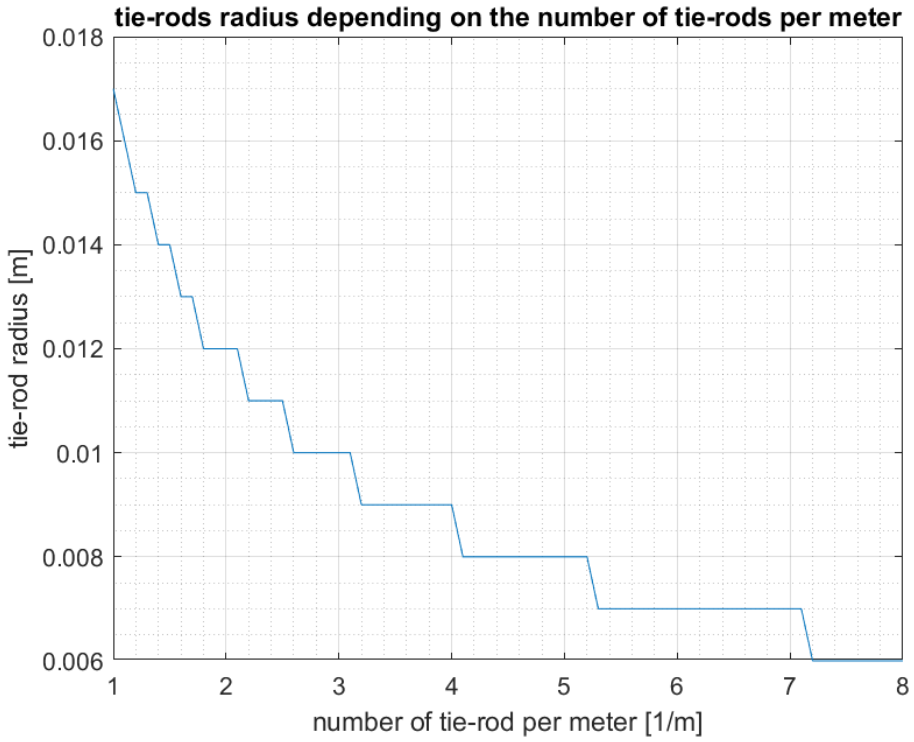

Figure 4.4: Tie-rods radius (integer number of mm) depending on the number of tie-rods per unit length.

The choice of the most suitable values for the radius will depends on the positions and configuration of the tie-rods, this will change their length and could change slightly its radius, different angle of connection will influence the value of the yielding stress. However, it was seen that for all the configurations considered the most reasonable value for the number of tie-rods per meter is 2.2, it is important to remember that the total number of tie-rods supporting the coils must be an integer.

Four tie-rods configurations where considered:

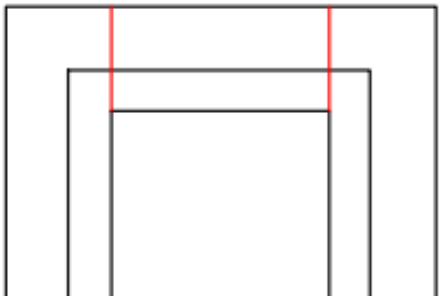

(a) Vertical configuration

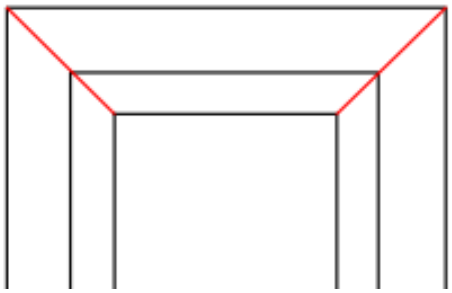

(b) Diagonal configuration

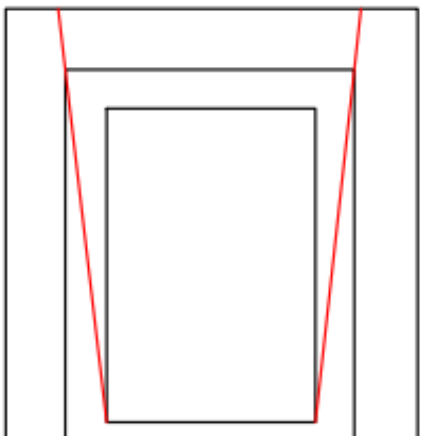

(c) Vertically crossed configuration

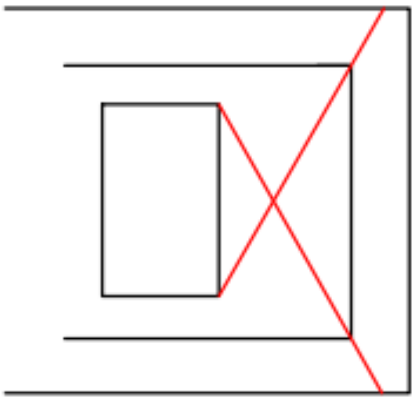

(d) Horizontally crossed configuration

Figure 4.5: Tie-rods configurations.

It is important to notice that the first three configurations consider the thermal shield as equally distant from the coils, instead the fourth will considered the thermal shield equally distant from the iron yoke, hence it will consider the actual area instead of the reduced one (Figure 4.1).

Coolers

The final number of cryocoolers highly influences the temperature profile and linear power density profile of the coils.

The two principal possibilities are to cool the system from one or two sides, respectively using 2 or 4 cryocoolers, obviously from the thermal analysis is better to cool from both ends to lower the maximum temperature reached inside the coil, but this is not always possible due to the presence in the gantry of particle trackers on one end of the magnet. From now on it will consider a system with two cooling sides but always considering the one side option. Moreover, it is proposed also a three-side option where it is introduced a bore at 2/3 of the length of the magnet in which are inserted two cooling heads, this option could solve the gantry-problem without increasing much the internal temperature. This last option must be studied more because introducing a hole in the iron yoke will highly influence the magnetic field, hence here it is just introduced as an idea for future studies.

For the cryocoolers, depending on the power output and according to the temperature boundaries, three possible cryocoolers model are considered. All three models are standard two-stage pulse tube cryocoolers from Cryomech [47].

When deciding which cryocoolers is the most suitable it is important to know the first and second stage temperatures and their respective extracted powers. In our model the first stage temperature is set at 60 K and the second stage temperature is set at 10 K. The choice of the cryocooler is very important due to their costs and dimensions, it is important to choose a cryocooler that will fit in the spacing, for example due to the grating, but it is also important to minimize the cost of them, usually a couple of cryocoolers are installed as backup to avoid failure and quenching of the magnet.

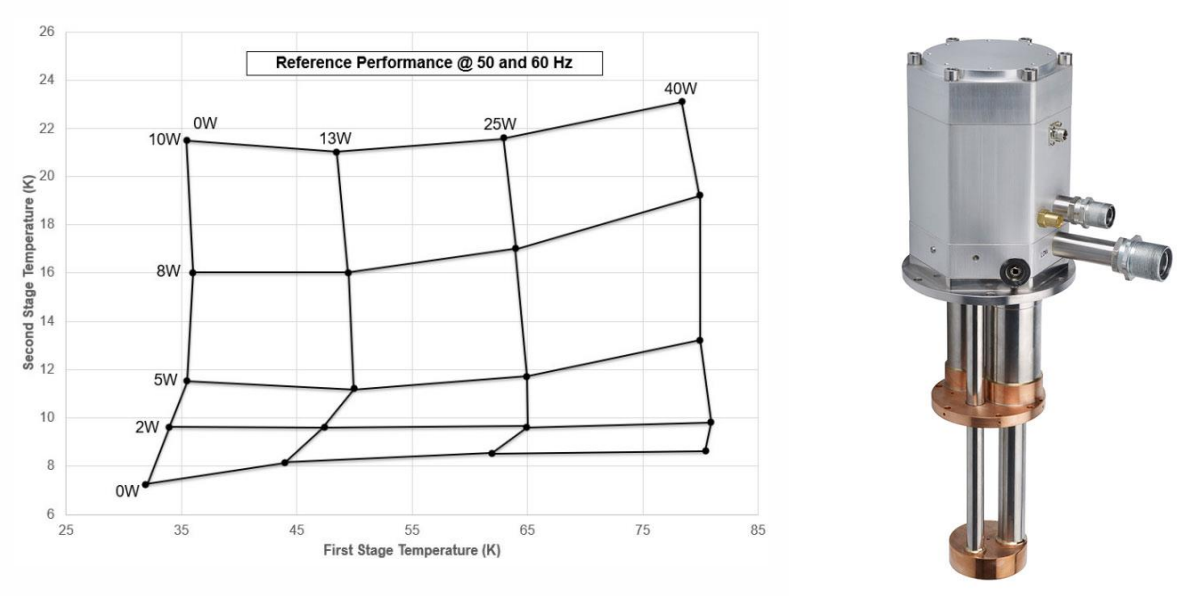

Figure 4.6: PT805 cryocooler (right) and its capacity curve (left).

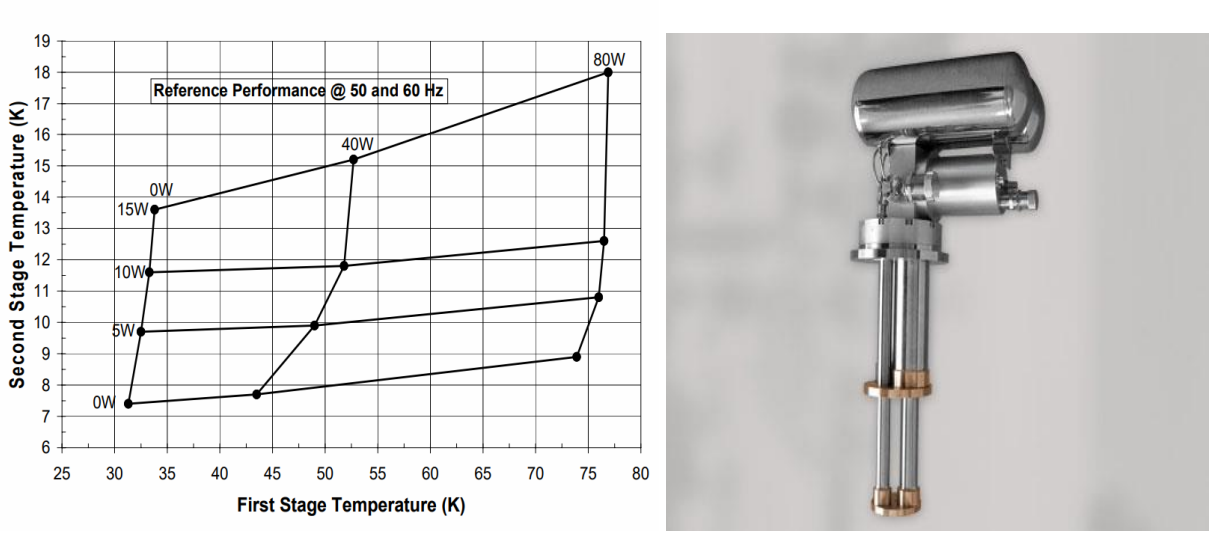

Figure 4.7: PT810 cryocooler (right) and its capacity curve (left).

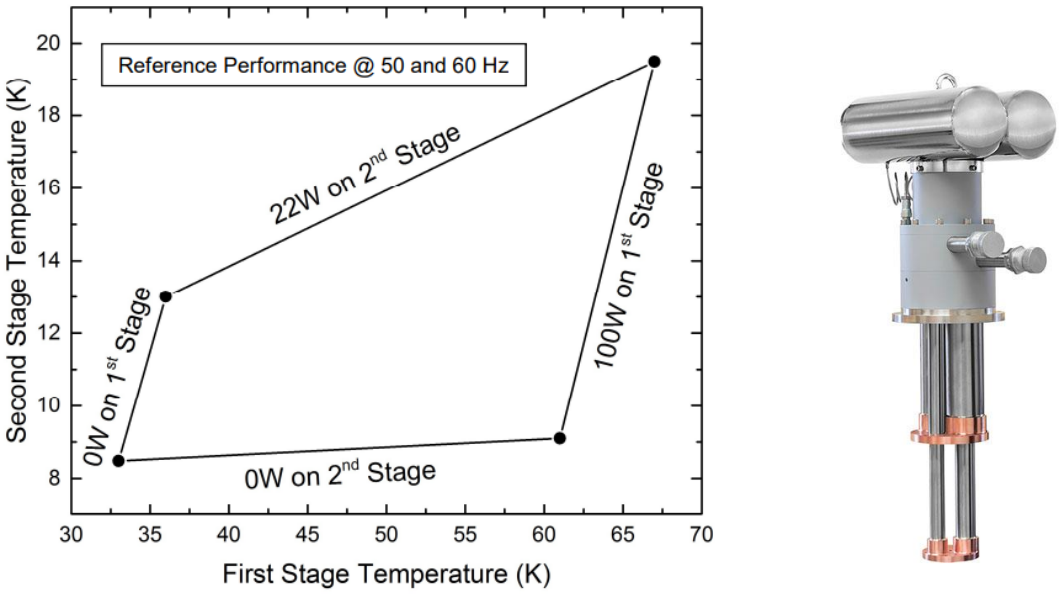

Figure 4.8: PT815 cryocooler (right) and its capacity curve (left).

Thermal shield

As said in section 3.3, the thermal shield has an important role in lowering the heat flux arriving on the coils. The material that constitutes the shield must have two properties: it must be relatively light, and it must have a high thermal conductivity at cryogenic temperatures. For these purposes were considered aluminum and copper, the first one lighter and the second one with a higher thermal conductivity.

Considering a sample configuration:

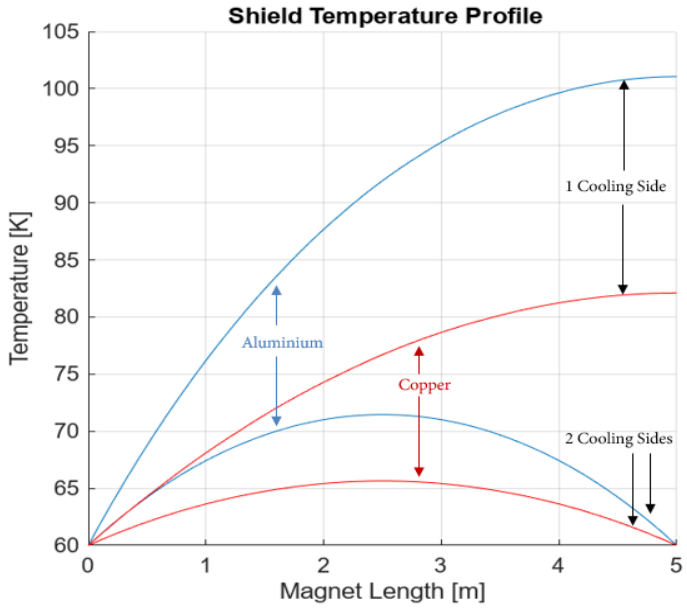

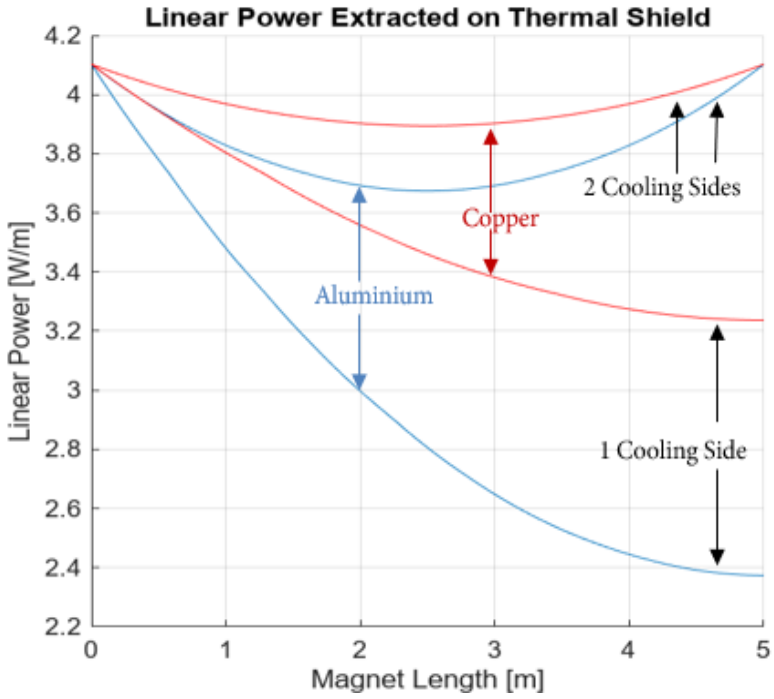

Figure 4.9: Thermal shield temperature profile (above) and linear power density profile (below).

From the Figure 4.9, it is evident that copper as a material is thermally more convenient, reaching a lower maximum temperature inside the shield.

Another important problem concerning the thermal shield is the presence of electrical current during the magnetic field transient, this current will generate additional power losses. One possible solution is to use different slabs of copper glued with epoxy resin instead of using a continuous slab. This adjustment will cut the current and should not change the thermal consideration of the shield itself. Further analyses are suggested to prove the availability of this solution.

Optimization over coils

It is important to stress that all the results and the considerations made have the goal of minimizing the thermal load and the linear power density on the coils. They are the most sensitive component of the system, due to their superconductive nature.

Regarding this matter it can be seen that the temperature profile of the thermal shield and the power losses inside the ropes have a central role. The first one will highly influence the heat flux arriving on the coils from the outside (equation (1.10)) and the second one will influence the coil temperature profile. Hence minimizing these two factors is a pivotal matter in finding the best solution.

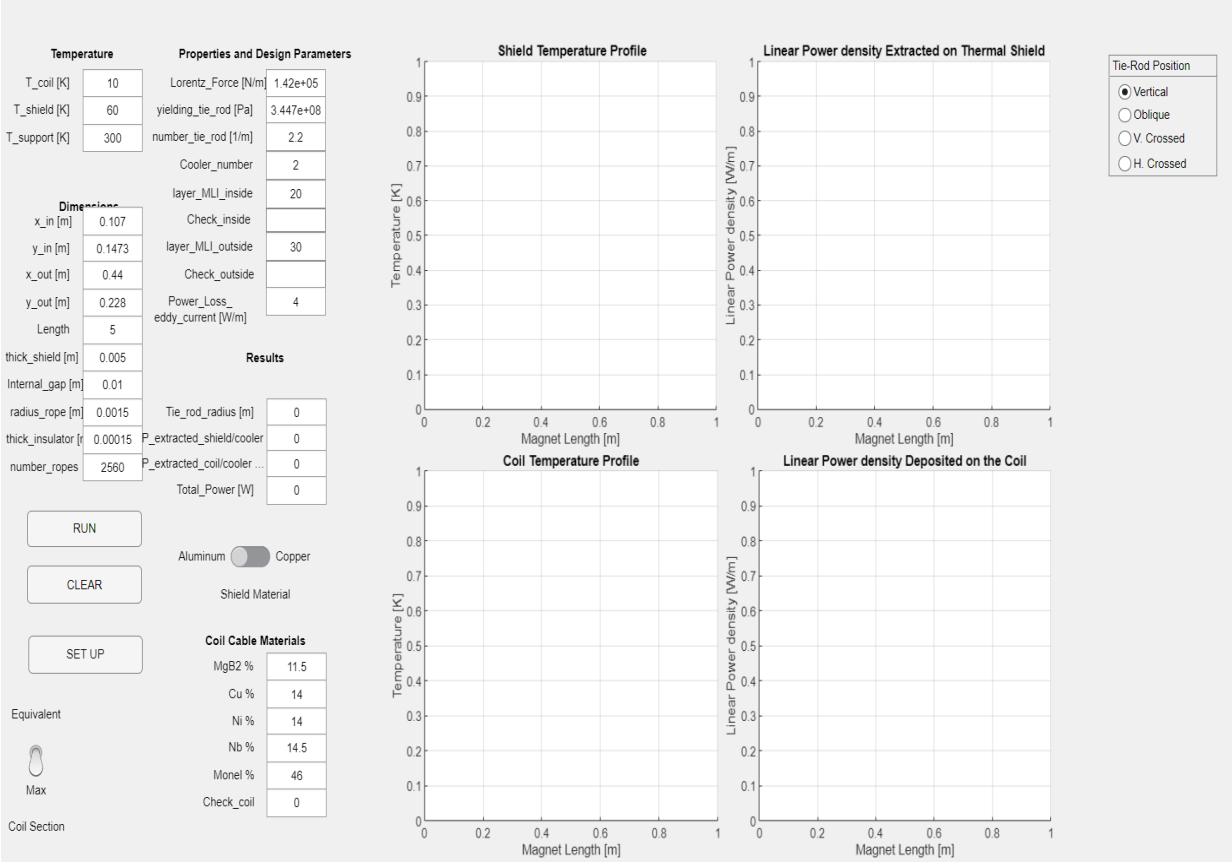

Figure 4.10: Visual interface of the thermal sub-model.

4.2.3 Current leads model

Current leads for cryogenic applications are designed to transmit large currents from room temperature to the very low temperatures of superconducting coils. Current leads that are good electrical conductors are also good conductors of heat, but for cryogenic applications, current leads must minimize heat in-leak whilst safely carrying the design current.

The goal of this model is to minimize heat in-leak in the magnet. To achieve the goal, it was designed the current lead with dimensions that generate a temperature profile inside the current leads with a zero-temperature derivative at the hot end and an infinite one at the cold end attached to the coils. In such a way no heat is leaked inside, once decided the physical boundaries conditions the dimensions were founded minimizing the power consumption by the current leads, always considering a total current of 276 A.

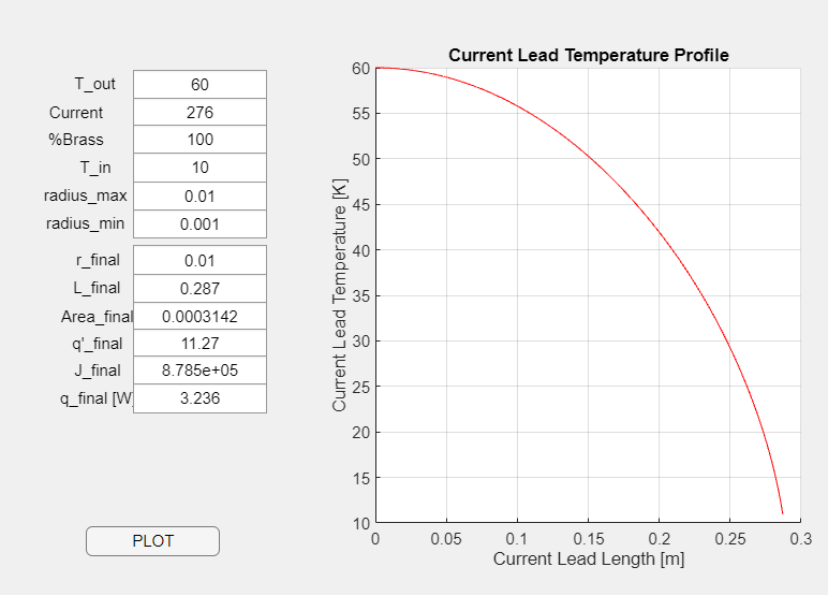

Figure 4.11: Visual interface of the current leads sub-model

Hot head

The hot head is constituted by a couple of resistive leads made by brass [51], they will bring the current from 300 K to 60 K.

The minimum power loss is:

$$P_{hot} = 13.88 \cdot 2 = 27.76\ W$$

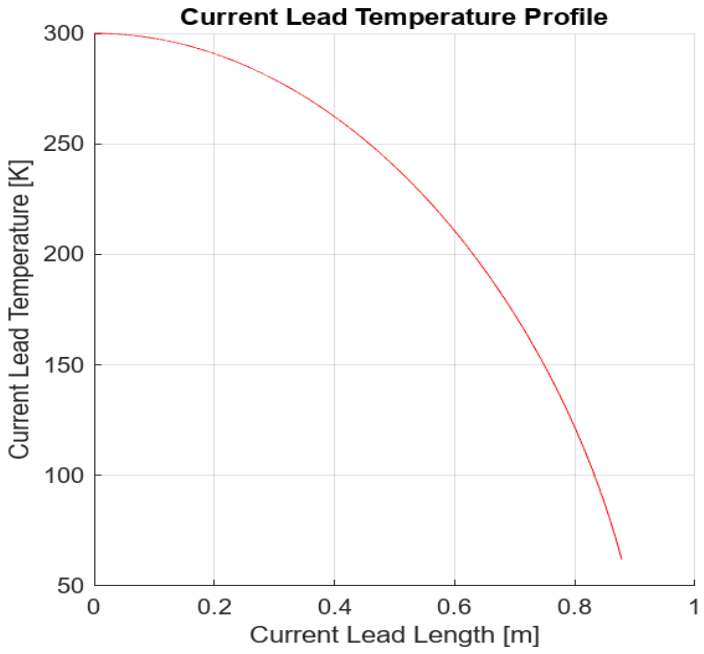

Figure 4.12: Temperature profile of the current leads in the hot head

	Radius	Area	Length	Current density	Maximum linear power density
Optimal dimensions	0.01 [m]	0.000314 [m^2]	0.878 [m]	8.78*10^5 [A/m^2]	15.81 [W/m]

Table 4.4: Hot head current leads dimensions

Cold head

For the cold head two possible couple of leads were considered to transmit the current form 60 K to 10 K:

- Couple of superconducting leads with loss:

$$P_{cold,SC} = 0.16\ W$$

- Couple of normal resistive leads made by brass with losses:

$$P_{cold,NR} = 3.236 \cdot 2 = 6.472\ W$$

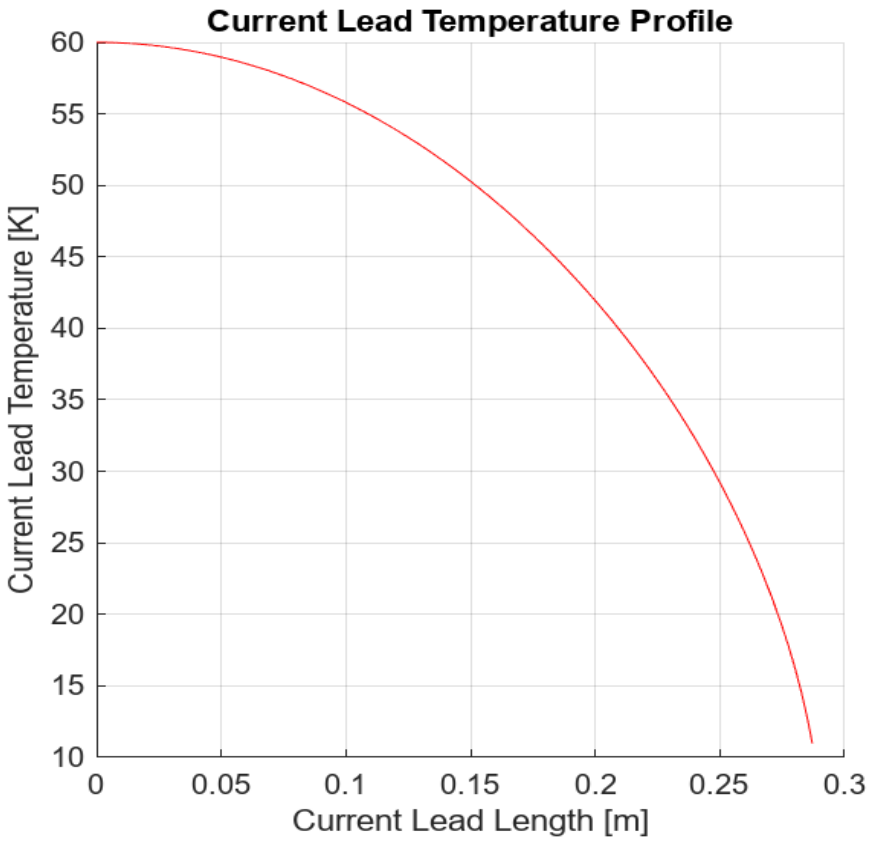

Figure 4.13: Temperature profile of the current leads in the cold head

	Radius	Area	Length	Current density	Maximum linear power density
Optimal dimensions	0.01 [m]	0.000314 [m^2]	0.287 [m]	8.785*10^5 [A/m^2]	11.27 [W/m]

Table 4.5: Cold head current leads dimensions

To have the lower power loss possible in the cold head will be considered the superconducting couple.

4.2.4 Enthalpy model

This last model was created to analyze, accordingly with Hypothesis 7, the number of maximum cycles the magnet can sustain before reaching the critical temperature.

Currently exists several models that considered power dissipation in superconductor, see [52]. They consider the magnetic hysteresis in superconducting materials, alongside the magnetic field, the magnetization is fundamental to obtain the power loss density. In this models are also considered the inter-filament and intra-filament contributions, considering an equivalent resistance inside or between the filaments to compute power losses. It is important to notice that the hysteretic one is 1-2 order of magnitude bigger than the intra and inter-filament, hence will be the main contribution in the AC losses.

In addition, it may also verify the possibility to lower the internal power losses and their dependance with the field and the number of ropes. Lastly, it considers a loosening of Hypothesis 7 and calculates what is the ratio of work time and rest time if the cryocoolers can extract some power during the ramp up or ramp down of the magnetic field.

Considering the maximum temperature reached inside the coils it was possible to derive the maximum number of cycles, this value does not consider possible degradation of work performances due to the temperature increase.

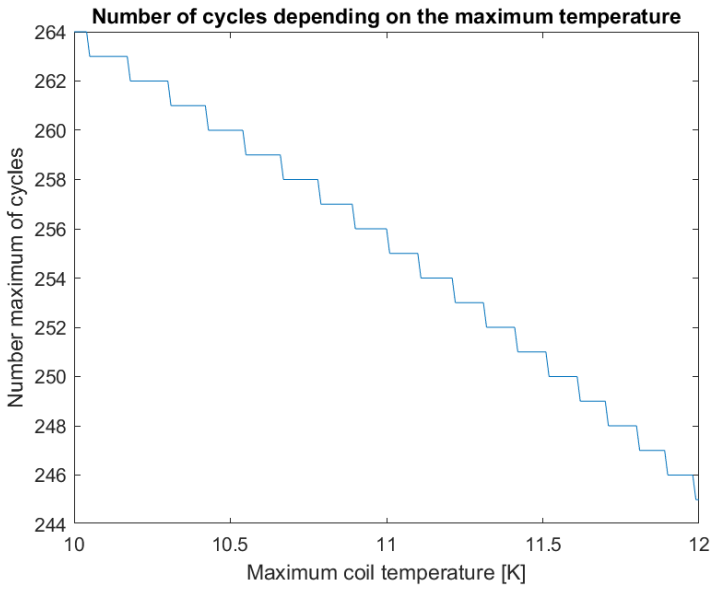

Figure 4.14: Number of cycles for which the temperature reaches the critical one.

AC losses

In a superconducting material the critical current density depends on the temperature of the material and magnetic field peak on the conductor. To avoid any instability, the system will work at a certain margin from the critical value, usually 40%. Hence, we could increase the temperature by decreasing the current density in the coils, therefore increasing the number of total ropes. The total number of ropes, alongside the magnetic field, also modify the internal power losses density.

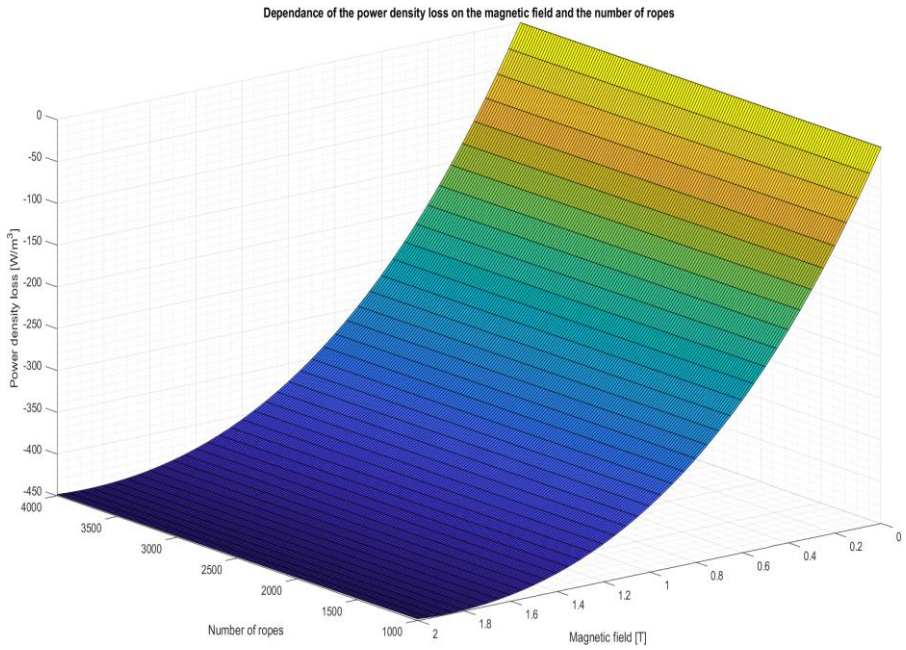

Figure 4.15: Power density loss.

As can be seen by the Figure 4.15, the most important factor is the magnetic field value, and will only slightly depend on the total number of ropes, The field maps, by changing the number of ropes, were approximated by considering the diameter of the coil and linearizing the field so that it was zero outside.. An assumption of scaling the magnetic field using a single field map was made. It can be deduced that it is more convenient to work with less ropes as possible, but this will worsen the work temperature as we can see from Figure 4.16:

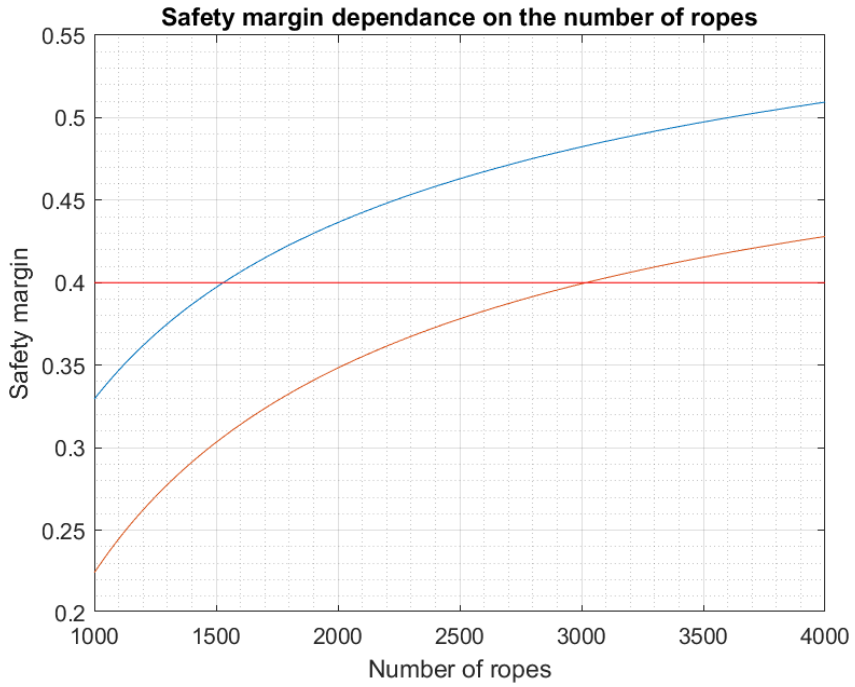

Figure 4.16: Work safety margin of the coil depending on the total number of the ropes at 10 K (blue) and 15 K (orange) with respect to the chosen margin at 0.4 (red).

It can be seen that increasing the number of ropes allows the possibility to work at higher temperatures with the same margin.

In conclusion, a good trade-off between working temperature and power losses must be achieved. In this model 1260 ropes where chosen as a first evaluation but future studies will be performed to obtain the optimal working point at different temperatures above at 10 K.

Idle work time

If we loosen the Hypothesis 7, it is possible that the cryocooler can extract some power during the duty cycle. Depending on the power extracted it is possible to define a ratio between work time and rest time required to have an initial condition after a work-rest sequence, this influences the choice of cryocooler and work possibility of the system.

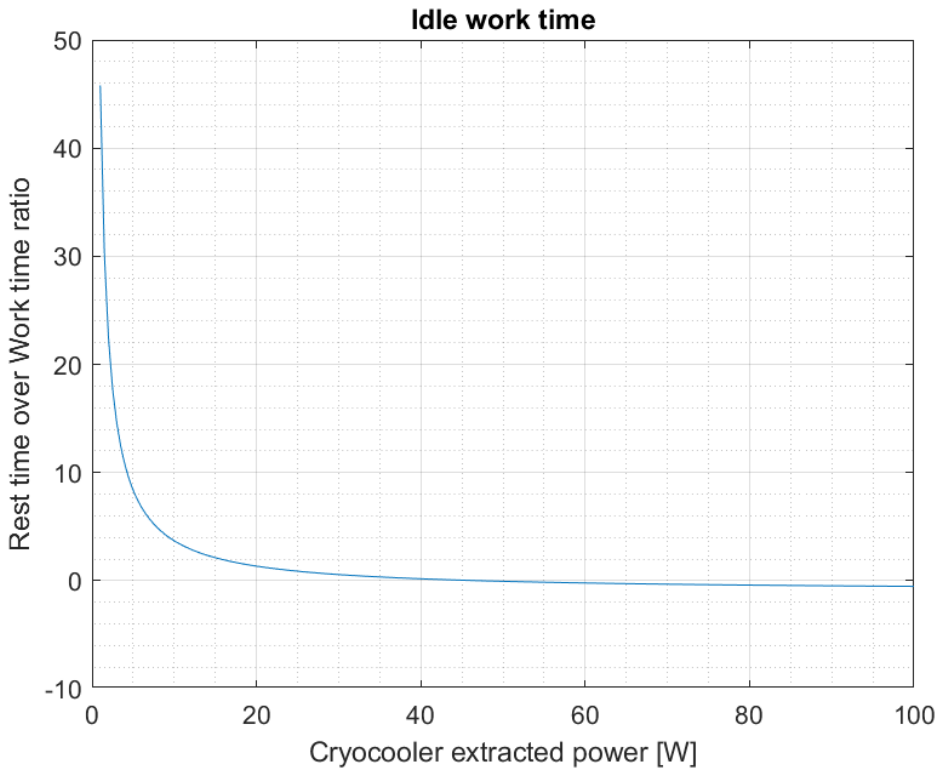

Figure 4.17: Rest time over work time depending on the instantaneous power extracted by the cryocooler, below zero no rest time required.

4.3 Results

In the final analysis, the most suitable conditions were considered. It was preferred to use:

- copper as thermal shield material;
- two sides cooling using compressively 4 cryocoolers for the coils cooling;
- 1260 total ropes, 630 for each coil;
- 11 total tie-rods;
- 20 MLI layers in the inner gap and 30 in the outer one.

With these initial conditions it was possible to analyze the temperature profile for each of the four tie-rods configurations and the total extracted power on the coils.

It is possible to notice how the (d) configuration of the tie-rods is the best one keeping a temperature profile quite low, this is due to the length of the tie-rods in the inner gap, reducing the conduction heat flux on the coils. Moreover, the (c) configuration is far from optimal, this is due to the high slop of the tie-rods that decrease sensitively the yield strength, hence from now on the (c) configuration will not be considered anymore, being the worst configuration analyzed.

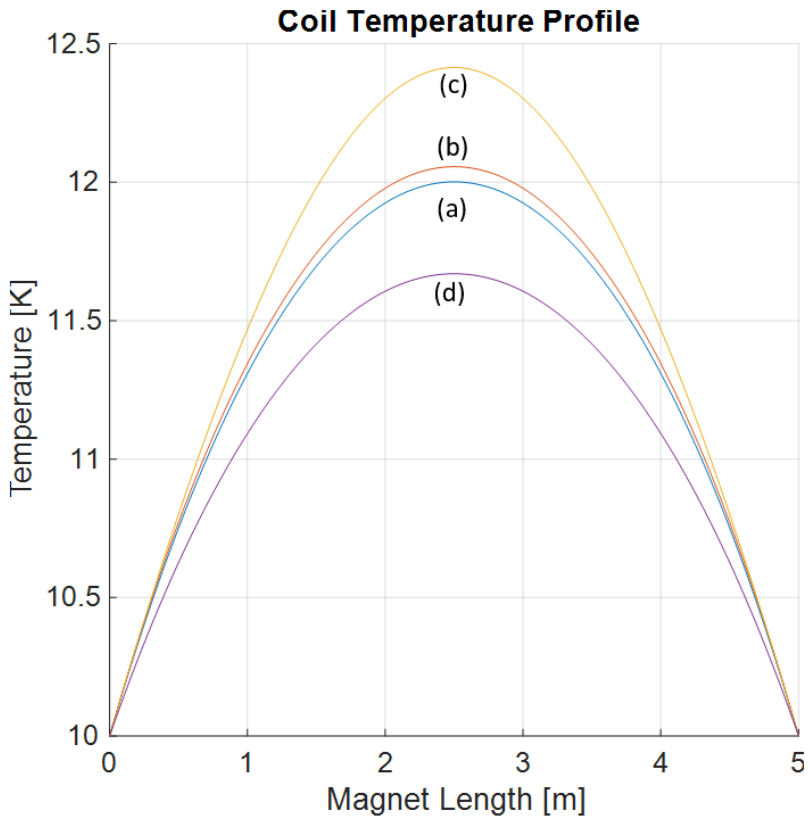

Figure 4.18: Temperature profile on the coils depending on the tie-rods configuration.

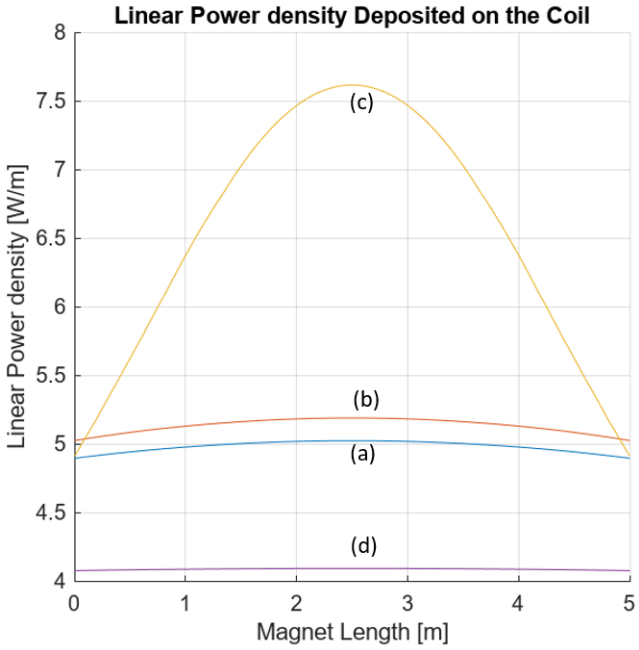

Figure 4.19: Linear power density on the coils depending on the tie-rods configuration.

	Extracted Energy per Cooler [W]	Maximum temperature [K]	Tie-rod radius [m]
(a)	12.45	12.0013	0.011
(b)	12.84	12.0561	0.014
(c)	16.41	12.4141	0.038
(d)	10.22	11.6695	0.014

Table 4.6: Significative results on coil analysis depending on the configuration.

The chosen configuration leads to a tie-rods radius of 0.014 mm and maximum temperature of 11.67 K. The configuration change also the temperature profile and the linear power density profile on the thermal shield.

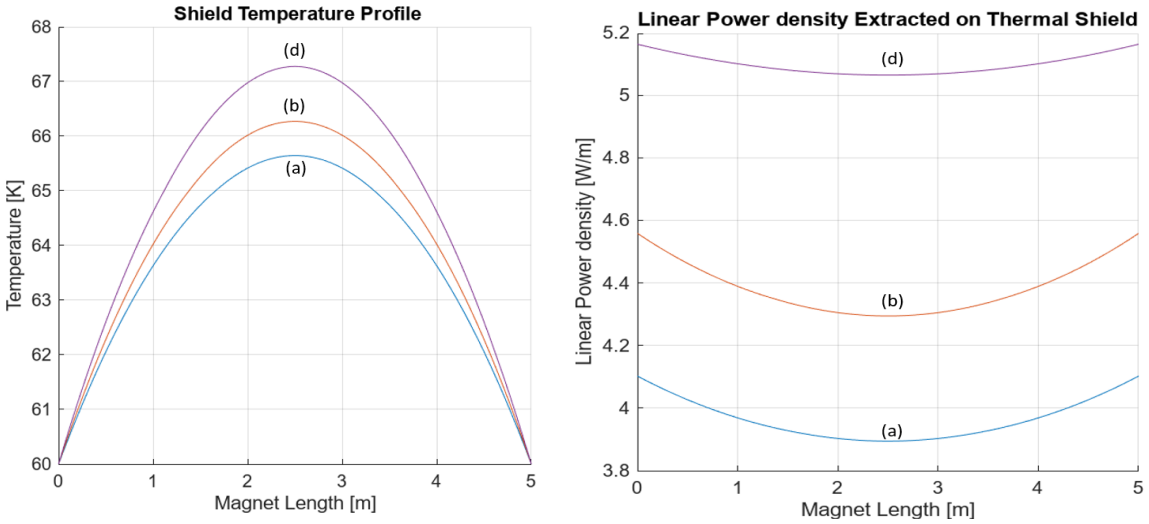

Figure 4.20: Linear power density on the shield (right) and temperature profile (left) depending on the tie-rods configuration.

It is important to remember that reducing the temperature on the thermal shield not always have a beneficial effect on the temperature profile of the coil, that will depend highly on the tie-rods length, see equation (1.10).

	Extracted Energy per Cooler [W]	Maximum temperature [K]
(a)	9.908	65.6468
(b)	10.96	66.2719
(d)	12.74	67.2767

Table 4.7: Thermal shield values obtained depending on the configuration.

Lastly, using (d) tie-rods configuration and a maximum temperature of 11.67 K, is possible to obtain the maximum value of cycle before reaching the critical temperature, the value obtained is 249.

For a further analysis, it is also possible to analyze how the values of maximum temperature and total extracted power changes while varying the number of cooling sides and cryocoolers, considering the same tie-rods configuration (d).

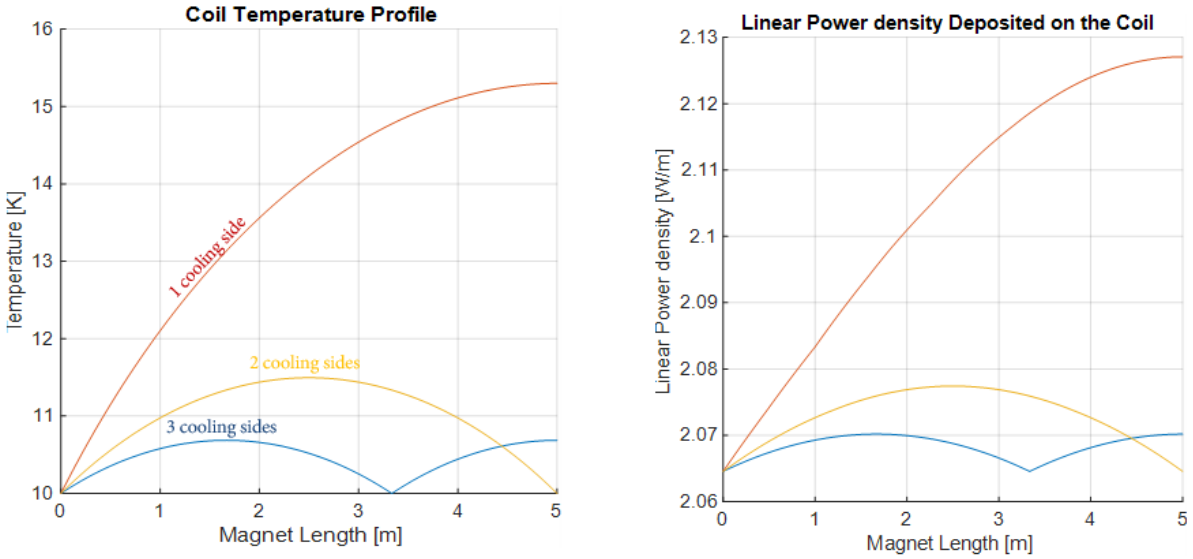

Figure 4.21: Linear power density (right) and temperature profile (left) of the coil depending on the number of cooling sides.

	Extracted Energy per cooler on the coils [W]	Extracted Energy per cooler on the shield [W]	Total power extracted [W]
1 cooling side	20.63	24.34	89.94
2 cooling sides	10.22	12.74	91.85
3 cooling sides	6.797	8.548	92.07

Table 4.8: Power extracted depending on the number of cooling sides.

As can be seen in Table 4.8, the two cooling sides configuration, if possible, is the most convenient without further modeling, having a low total extracted power and a low maximum temperature reached inside the coils.

5. Conclusion and Future Developments

This analysis is focused on optimizing the thermal transfer and power consumption of a magnet system by substituting normal conducting magnets with superconducting ones. The main goal is to reduce the power consumed by the magnet by a factor of 5-10, which would result in significant energy savings and potentially expand the use of the accelerator for medical purposes. Various factors were considered such as temperature boundary conditions, dimensions of the coils and thermal shield, composition and dimensions of the ropes, Lorentz force, tie-rods configuration, number of cooling sides, layers of MLI, and AC losses due to eddy currents.

Several important results were obtained:

- MgB_2: It was found out that MgB_2, with the proper design, can be efficiently used as coils' material without much thermal and operational constrains, in addition to its relatively low cost.
- Temperature and power density profiles: The goal is to minimize the thermal load and linear power density on the coils, which are crucial for superconducting operation. In the configuration chosen $10.22\ W$ per cryocooler were extracted from the coil and $12.74\ W$ on the thermal shield.
- Dimension Optimization: The analysis considers the optimization of various dimensions, such as the gaps between the coils and yoke, thickness of the thermal shield, radius of tie-rods, and dimensions of current leads. These optimizations aim to minimize heat flux, power losses, and heat in-leak, while ensuring the safe and efficiency of the magnet. Important considerations are the tie-rods design ((d) see Figure 4.5), the thermal shield thickness of 5 mm and the internal gap one of 10 mm. It is important to notice also the use of MLI around the thermal shield and the coils.
- Cryocooler Selection: The model evaluates different cryocooler options based on their power output, first and second stage temperatures, and extracted powers. Regarding the extracted power on the coils, it has been decided to use four cryocoolers PT815 with a consumption during the duty-cycle of $9.2\ kW$.

Instead, due to the power extracted from the current leads (0.16 W at the cold head and 27.76 W at the hot head) it was decided to utilize two PT805 with power on the duty-cycle of 5.4 kW each. It is important to notice that each compressor needs a water chiller each consuming 1.47 kW approximately, depends on the chosen chiller model [48].

– Material Selection: The thermal shield material is considered crucial for minimizing heat flux and temperature rise. The analysis compares materials like aluminum and copper, considering their thermal conductivity and weight. Copper is found to be more thermally favorable, reaching lower maximum temperature.

Nowadays the CNAO facility consume almost 30 kW in DC current averaged over a year. Depending on the work ratio the average power consumed over a year changes, it is possible to notice that with a work ratio lower than 0.53 it is possible to have an improvement of the overall consumption.

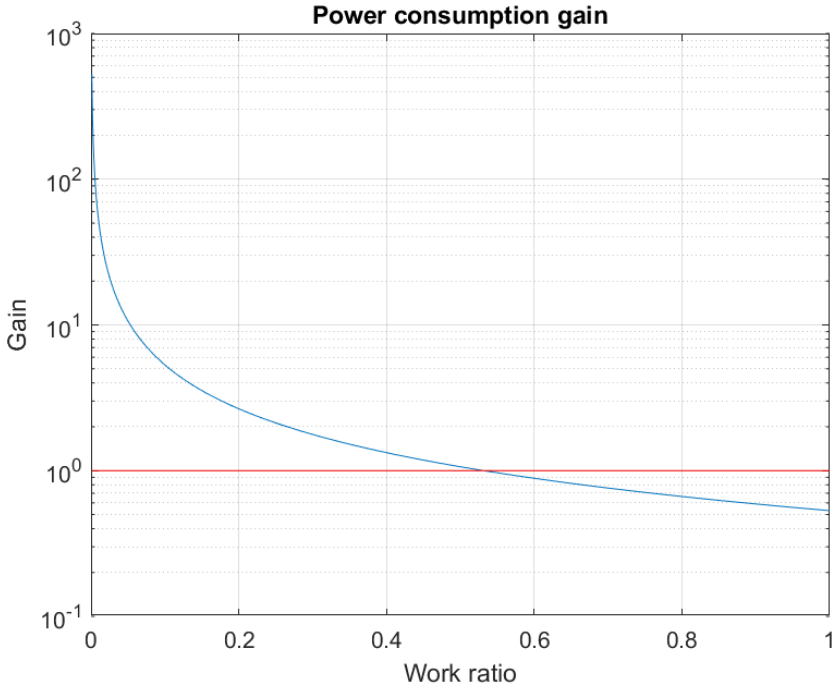

Figure 5.1: Power Consumption gain of the superconducting magnet over the resistive one (blue) compared to the normal resistive one (red).

Some possible areas for further development and analysis could include:

– Magnetic Field Considerations: The analysis could incorporate a detailed examination of the magnetic field properties, considering the impact of the magnet's bend and its interaction with the surrounding environment. This could help refine the model and provide more accurate results.

- Validation and Experimental Verification: To validate the model's predictions and assumptions, experimental tests could be conducted on a prototype or existing magnet system. The experimental data can be compared with the model's outputs to verify the accuracy and reliability of the analysis.
- Cost Optimization: In addition to energy savings, it would be valuable to consider the cost implications of implementing superconducting magnets. Further analysis could explore the economic feasibility and return on investment associated with the proposed magnet system, considering factors such as initial investment, operational costs, and potential benefits.
- Magnet material: several other materials for the superconducting cable construction can be considered, such as ReBCO tapes.
- System Integration: The analysis could be expanded to include a more comprehensive examination of the entire magnet system, including the integration of the superconducting magnet with other components such as power supplies, cooling systems, and control systems. This holistic approach would provide a more complete understanding of the overall system performance and optimization opportunities.
- Reliability and Safety Analysis: A thorough assessment of reliability and safety aspects should be conducted to identify potential failure modes, assess risk factors, and design appropriate safety measures. This analysis would ensure the safe operation of the magnet system and mitigate any potential risks associated with superconducting technology.

It is important to note that the above suggestions are based on the preliminary information obtained during the analysis. Further details and specific requirements of the magnet system would be necessary to conduct a more comprehensive analysis and suggest more precise areas for further development.

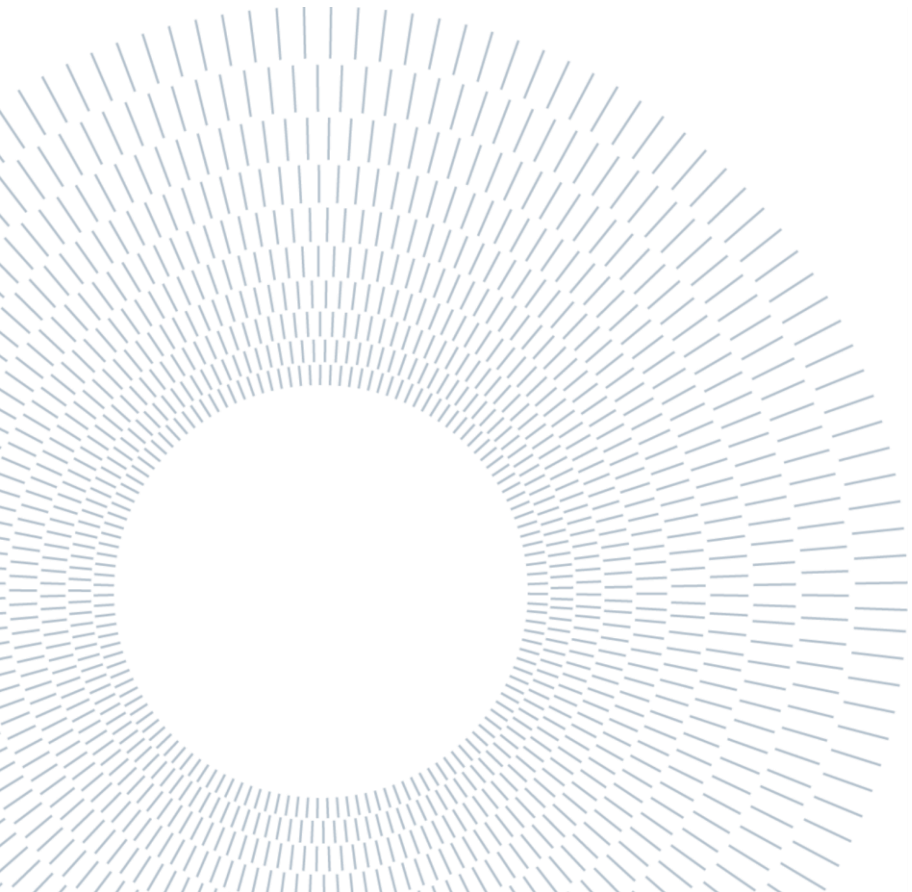

Bibliography

[1] A. Abada *et al.*, "FCC-hh: The Hadron Collider: Future Circular Collider Conceptual Design Report Volume 3," *European Physical Journal: Special Topics*, vol. 228, no. 4, pp. 755–1107, Jul. 2019, doi: 10.1140/epjst/e2019-900087-0.

[2] G. Bisoffi, E. Benedetto, M. Karppinen, M. R. Khalvati, R. Van Weelderen, and M. Sapinski, "Energy Comparison of Room Temperature and Superconducting Synchrotrons for Hadron Therapy," 2022, doi: 10.18429/JACoW-IPAC2022-THPOMS049.

[3] D. Halliday and R. Resnick, *Fundamentals of Physics*. 2013.

[4] P. Duthil, "Material Properties at Low Temperature."

[5] E. D. Marquardt, J. P. Le, and R. Radebaugh, "Cryogenic Material Properties Database Cryogenic Material Properties Database," 2000.

[6] C. Kittel, *Introduction to Solid State Physics*. 2005.

[7] P. Debye, "Zur Theorie der spezifischen Wärmen," *Ann Phys*, vol. 344, no. 14, pp. 789–839, Jan. 1912, doi: 10.1002/andp.19123441404.

[8] M. Trojan, "One-Dimensional, Steady-State Heat Conduction," in *Encyclopedia of Thermal Stresses*, R. B. Hetnarski, Ed., Dordrecht: Springer Netherlands, 2014, pp. 3483–3498. doi: 10.1007/978-94-007-2739-7_401.

[9] H. Ibach and H. Lüth, *Solid-State Physics*. Berlin, Heidelberg: Springer Berlin Heidelberg, 2009. doi: 10.1007/978-3-540-93804-0.

[10] R. Franz and G. Wiedemann, "Ueber die Wärme-Leitungsfähigkeit der Metalle," *Annalen der Physik und Chemie*, vol. 165, no. 8, pp. 497–531, Jan. 1853, doi: 10.1002/andp.18531650802.

[11] O. Darrigol, *Electrodynamics from Ampere to Einstein*. 2000.

[12] E. Grüneisen, "Die Abhängigkeit des elektrischen Widerstandes reiner Metalle von der Temperatur," *Ann Phys*, vol. 408, no. 5, pp. 530–540, Jan. 1933, doi: 10.1002/andp.19334080504.

[13] J. W. Ekin, *Experimental Techniques for Low-Temperature Measurements Cryostat Design, Material Properties, and Superconductor Critical-Current Testing*. 2006.

[14] G. K. White, "Experimental Techniques in Low-Temperature." p. 319, 1987.

[15] A. Bui, "Techniques de l'ingénieur B," no. 2, 1993.

[16] R. Rahemi and D. Li, "Variation in electron work function with temperature and its effect on the Young's modulus of metals," *Scr Mater*, vol. 99, pp. 41–44, 2015, doi: 10.1016/j.scriptamat.2014.11.022.

[17] S. J. Blundell, "Magnetism in Condensed Matter," 2001.

[18] E. Lenz, "Richtungsmessungen von Ultrastrahlungsteilchen auf dem Jungfraujoch," *Ann Phys*, vol. 421, no. 8, pp. 741–757, Jan. 1937, doi: 10.1002/andp.19374210807.

[19] A. Matthiessen and M. von Bose, "I. On the influence of temperature on the electric conducting power of metals," *Philos Trans R Soc Lond*, vol. 152, pp. 1–27, Dec. 1862, doi: 10.1098/rstl.1862.0001.

[20] K. Onnes, "Further experiments with liquid helium. C. On the change of electric resistance of pure metals at very low temperatures etc. IV. The resistance of pure mercury at helium temperatures," 1911. [Online]. Available: http://www.digitallibrary.nl'

[21] J. F. Annett, "Superconductivity, Superfluids and Condensates," 2003.

[22] Philippe. Mangin and R. Kahn, *Supraconductivité : introduction*. EDP Sciences, 2013.

[23] A. P. Drozdov, M. I. Eremets, I. A. Troyan, V. Ksenofontov, and S. I. Shylin, "Conventional superconductivity at 203 kelvin at high pressures in the sulfur hydride system," *Nature*, vol. 525, no. 7567, pp. 73–76, 2015, doi: 10.1038/nature14964.

[24] J. G. Bednorz and K. A. Müller, "Possible highTc superconductivity in the Ba−La−Cu−O system," *Zeitschrift für Physik B Condensed Matter*, vol. 64, no. 2, pp. 189–193, 1986, doi: 10.1007/BF01303701.

[25] W. Meissner and R. Ochsenfeld, "Ein neuer Effekt bei Eintritt der Supraleitfähigkeit," *Naturwissenschaften*, vol. 21, no. 44, pp. 787–788, 1933, doi: 10.1007/BF01504252.

[26] H. L. Stormer and D. C. Tsui, "The Quantized Hall Effect," *Science (1979)*, vol. 220, no. 4603, pp. 1241–1246, Jun. 1983, doi: 10.1126/science.220.4603.1241.

[27] F. London, *Superfluids: Vol I Macroscopic Theory of Superconductivity*, 2nd ed., vol. 1. 1960.

[28] A. A. Abrikosov, "On the Magnetic Properties of Superconductors of the Second Group," *J, Exptl. Theoret. Phys. (U.S.S.R.)*, vol. 5, no. 6, pp. 1174–1182, 1954.

[29] N. Haleeda, M. Awang Kechik, and R. Abd-Shukor, "Effect of Yb2O3 Nanoparticle Addition on Superconducting Properties of BSCCO (2223)/Ag Tapes by Acetate Precipitation Method," *Pertanika J Sci Technol*, vol. 2, Jan. 2016.

[30] R. P. Huebener, "The Abrikosov Vortex Lattice: Its Discovery and Impact," *J Supercond Nov Magn*, vol. 32, no. 3, pp. 475–481, 2019, doi: 10.1007/s10948-018-4916-0.

[31] F. London, H. London, and F. A. Lindemann, "The electromagnetic equations of the supraconductor," *Proc R Soc Lond A Math Phys Sci*, vol. 149, no. 866, pp. 71–88, Jan. 1935, doi: 10.1098/rspa.1935.0048.

[32] C. J. Gorter and H. Casimir, "On supraconductivity I," *Physica*, vol. 1, no. 1, pp. 306–320, 1934, doi: 10.1016/S0031-8914(34)90037-9.

[33] J. Bardeen, L. N. Cooper, and J. R. Schrieffer, "Theory of Superconductivity," *Physical Review*, vol. 108, no. 5, pp. 1175–1204, Dec. 1957, doi: 10.1103/PhysRev.108.1175.

[34] D J Amit, "The Ginzburg criterion-rationalized," *Journal of Physics C: Solid State Physics*, vol. 7, no. 18, p. 3369, 1974, doi: 10.1088/0022-3719/7/18/020.

[35] V. L. Ginzburg and L. D. Landau, "On the Theory of superconductivity," *Zh. Eksp. Teor. Fiz.*, vol. 20, pp. 1064–1082, 1950, doi: 10.1016/B978-0-08-010586-4.50035-3.

[36] E. van Heumen *et al.*, "Optical and thermodynamic properties of the high-temperature superconductor HgBa2Ca2Cu3O8+δ," *Phys Rev B*, vol. 75, no. 5, p. 54522, Feb. 2007, doi: 10.1103/PhysRevB.75.054522.

[37] T. Matsushita, *Flux Pinning in Superconductors*. Berlin, Heidelberg: Springer Berlin Heidelberg, 2007. doi: 10.1007/978-3-540-44515-9.

[38] T. Matsushita, N. Ihara, and M. Kiuchi, "Flux Pinning Characteristics and Irreversibility Line in High Temperature Superconductors."

[39] J. Nagamatsu, N. Nakagawa, T. Muranaka, Y. Zenitani, and J. Akimitsu, "Superconductivity at 39 K in magnesium diboride," *Nature*, vol. 410, no. 6824, pp. 63–64, 2001, doi: 10.1038/35065039.

[40] A. R. Villagracia, "First principle investigation of atomic hydrogen adsorption on Pd-doped MgB2," *Philipp Sci Lett*, vol. 6, pp. 176–181, Oct. 2013.

[41] J. D. Jorgensen, D. G. Hinks, and S. Short, "Lattice properties of MgB2 versus temperature and pressure," *Phys Rev B*, vol. 63, no. 22, p. 224522, May 2001, doi: 10.1103/PhysRevB.63.224522.

[42] J. Kortus, I. I. Mazin, K. D. Belashchenko, V. P. Antropov, and L. L. Boyer, "Superconductivity of Metallic Boron in MgB2," *Phys Rev Lett*, vol. 86, no. 20, pp. 4656–4659, May 2001, doi: 10.1103/PhysRevLett.86.4656.

[43] Y. Wang, T. Plackowski, and A. Junod, "Specific heat in the superconducting and normal state (2–300 K, 0–16 T), and magnetic susceptibility of the 38 K superconductor MgB2: evidence for a multicomponent gap," *Physica C Supercond*, vol. 355, no. 3, pp. 179–193, 2001, doi: 10.1016/S0921-4534(01)00617-7.

[44] L. Rossi, S. Mariotto, and S. Sorti, "'Energy Saving Magnets for Beam Lines,'" in *IOP IPAC23*, 2023.

[45] M. Pruteanu, A. Radu, A. Ciobanu, and A. Iacob, *A closer examination of the thermal performance of Multifoil Insulations*. 2011.

[46] N. Almtireen, J. J. Brandner, and J. G. Korvink, "Pulse Tube Cryocooler: Phasor Analysis and One-Dimensional Numerical Simulation," *J Low Temp Phys*, vol. 199, no. 5, pp. 1179–1197, 2020, doi: 10.1007/s10909-020-02378-6.

[47] "https://www.cryomech.com/cryocoolers/pulse-tube-cryocoolers/."

[48] "http://www.frigosystem.it/refrigeratori-d-acqua/raca-c."

[49] T. Miyakita, R. Hatakenaka, H. Sugita, M. Saitoh, and T. Hirai, "Evaluation of Thermal Insulation Performance of a New Multi-Layer Insulation with Non-Interlayer-Contact Spacer," 2015.

[50] H. Tresca, "Mémoire sur l'écoulement des corps solides soumis à de fortes pressions.," *C. R. Acad. Sci. Paris*, vol. 59, p. 29, 1864.

[51] P. Arakawa, K. Efferson, and Y. Iwasa, "Helium vapor-cooled brass current leads: Experimental and analytical results," *Cryogenics (Guildf)*, vol. 41, pp. 485–489, Jun. 2001, doi: 10.1016/S0011-2275(01)00115-1.

[52] J. Hull *et al.*, "Superconducting Magnets," in *Applied Superconductivity: Handbook on Devices and Applications*, 2015, pp. 403–602. doi: 10.1002/9783527670635.ch4.

List of Figures

List of Tables

Acknowledgements

I would like to express my heartfelt gratitude to all my fantastic supervisors at PoliMi, INFN, and ASG. I can never thank them enough.
I would like to thank Alessio Capelluto, who helped me break out of my shell and exposed me to the early stages of this work, guiding me towards a path that I became passionate about. He provided an engineering perspective and was there for me until the very end.
I would like to thank Samuele Mariotto, who supported me during the most delicate moments. He has always been there and reignited my passion for what I do and study in a stimulating way. This thesis would never have been possible without him.
I would like to thank Matteo Passoni, who served as a beacon in this work and instilled his passion for what we study.
And I would like to thank all the employees/professors at Politecnico di Milano, INFN, and the University of Milan for accompanying me on this adventure.
I would like to express my gratitude to all my friends who have accompanied me on this journey, from the friends with whom I share everything since elementary school, to the high school classmates who have become lifelong friends, to the colleagues in physical and nuclear engineering with whom I shared so much, including a passion for physics. And a thank you to all those people who may have drifted away over the years but played a role in my growth.
I would like to thank my father, Fabrizio, and my mother, Michela, who have stimulated and supported my passion since I was a child. They have been by my side, as only they know how, through difficult, dark, or heavy moments. They have always been there, and I know I can always rely on them. I would like to thank my sister Sara, to whom I have always been close, and I hope to be there for her as she has been for me. And of course, I would like to thank my entire family: Grandpa Gianluca, Grandma Gabriella, Aunt Barbara, and Grandpa Gerardo, who raised me and with whom I cherish and will forever cherish beautiful memories.

Lastly, I want to thank Jessica, the person with whom I have shared every single thought and day during this challenging journey. She has been my guiding light and has helped me overcome anything. I will never stop thanking her enough because if I am where I am, it is also thanks to her. Thank you.

Simone Busatto